nature medicine

ARTICLES

https://doi.org/10.1038/s41591-022-02003-x

Check for updates

KIR-based inhibitory CARs overcome CAR-NK cell trogocytosis-mediated fratricide and tumor escape

Ye Li[1,2], Rafet Basar[1], Guohui Wang[1], Enli Liu[1], Judy S. Moyes[1], Li Li[1], Lucila N. Kerbauy[1,3,4], Nadima Uprety[1], Mohsen Fathi[5], Ali Rezvan[5], Pinaki P. Banerjee[1], Luis Muniz-Feliciano[1], Tamara J. Laskowski[1], Emily Ensley[1], May Daher[1], Mayra Shanley[1], Mayela Mendt[1], Sunil Acharya[1], Bin Liu[1], Alexander Biederstädt[1,6], Hind Rafei[1], Xingliang Guo[1], Luciana Melo Garcia[1], Paul Lin[1], Sonny Ang[1], David Marin[1], Ken Chen[7], Laura Bover[8,9], Richard E. Champlin[1], Navin Varadarajan[5], Elizabeth J. Shpall[1] and Katayoun Rezvani[1]✉

Trogocytosis is an active process that transfers surface material from targeted to effector cells. Using multiple in vivo tumor models and clinical data, we report that chimeric antigen receptor (CAR) activation in natural killer (NK) cells promoted transfer of the CAR cognate antigen from tumor to NK cells, resulting in (1) lower tumor antigen density, thus impairing the ability of CAR-NK cells to engage with their target, and (2) induced self-recognition and continuous CAR-mediated engagement, resulting in fratricide of trogocytic antigen-expressing NK cells (NK^{TROG+}) and NK cell hyporesponsiveness. This phenomenon could be offset by a dual-CAR system incorporating both an activating CAR against the cognate tumor antigen and an NK self-recognizing inhibitory CAR that transferred a 'don't kill me' signal to NK cells upon engagement with their $TROG^{+}$ siblings. This system prevented trogocytic antigen-mediated fratricide, while sparing activating CAR signaling against the tumor antigen, and resulted in enhanced CAR-NK cell activity.

Trogocytosis involves the rapid transfer of intact cell-surface proteins between cells and is induced by receptor–antigen ligation[1–4]. Trogocytosis is well-documented in leukocytes, including T cells and NK cells, and influences the response of the accepting cells, both positively and negatively[1,4–7]. Indeed, transfer of target antigen from the tumor cell surface to CAR-expressing T (CAR-T) cells through trogocytosis has been shown to contribute to antigen reduction and antigen-low tumor relapse in preclinical models[8].

NK cells are innate immune cells that mediate strong antitumor activity[9–11]. Unlike T cells, NK cells target cancer cells in a non-antigen-dependent manner, and their allogeneic use for adoptive cell therapy is not associated with graft-versus-host-disease[12–14]. Trogocytosis has been reported to regulate NK cell responses in different contexts and is mediated by the ligation of NK cell-activating receptors such as the natural cytotoxicity receptors and NKG2s with their cognate ligands[15–19].

Here, we used multiple in vivo tumor models and clinical samples to show that CAR activation promoted trogocytosis that, in turn, contributed to a reduction in antigen density on the tumor targets and loss of tumor control in vivo after CAR-NK cell therapy. Acquisition of the cognate tumor antigen by CAR-NK cells led to induced self-recognition and sustained CAR activation, but also decreased NK cell activity by driving fratricide and hyporesponsiveness. To overcome self-recognition of trogocytic antigen (TROG-antigen)-expressing ($TROG^{+}$) NK cells by the activating CAR (aCAR), we designed an inhibitory CAR (iCAR) against an NK-specific antigen by harnessing the physiological human leukocyte antigen (HLA)-restricted inhibitory signals that normally dampen NK cell function[20–23]. NK cells that expressed both an aCAR and an iCAR (AI-CARs) transferred a 'don't kill me' signal to NK cells upon recognition of the NK self-antigen, thus preventing fratricide and exhaustion mediated by the aCAR against NK^{TROG+} sibling cells, while sparing their activity against tumor cells, resulting in superior in vivo antitumor efficacy.

Our finding that trogocytosis negatively impacts the antitumor activity of CAR-NK cells may have important therapeutic implications that could be overcome using rationally designed AI-CAR systems that prevent trogocytic-antigen-induced on-target off-tumor effects while sparing their on-target antitumor activity.

Results

CAR-mediated TROG-antigen transfer to NK cells. Trogocytosis triggered by receptor–ligand interactions is a well-described phenomenon in NK cells[1,2,4]. Thus, we first asked whether an engineered

[1]Department of Stem Cell Transplantation and Cellular Therapy, The University of Texas MD Anderson Cancer Center, Houston, TX, USA. [2]UTHealth Graduate School of Biomedical Sciences, The University of Texas MD Anderson Cancer Center, Houston, TX, USA. [3]Human Genome and Stem Cell Research Center, Department of Genetics and Evolutionary Biology, Biosciences Institute, University of Sao Paulo, Sao Paulo, Brazil. [4]Department of Stem Cell Transplantation and Cellular Therapy, Hospital Israelita Albert Einstein, Sao Paulo, Brazil. [5]Department of Chemical and Biomolecular Engineering, University of Houston, Houston, TX, USA. [6]Department of Medicine III: Hematology and Oncology, Technical University of Munich, Munich, Germany. [7]Department of Bioinformatics and Computational Biology, The University of Texas MD Anderson Cancer Center, Houston, TX, USA. [8]Department of Genomic Medicine, The University of Texas MD Anderson Cancer Center, Houston, TX, USA. [9]Department of Immunology, The University of Texas MD Anderson Cancer Center, Houston, TX, USA. ✉e-mail: KRezvani@mdanderson.org

activating receptor such as anti-CD19 CAR (CAR19) can also mediate the transfer of its cognate antigen, CD19, to NK cells following coculture with Raji^{CD19+} lymphoma cells. Nontransduced NK (NT-NK) cells and those expressing 19scFv (anti-CD19 CAR lacking all intracellular domains) were used as parental control and receptor control, respectively. Within minutes of coculture with Raji targets, a significantly greater percentage (75 ± 10%) of CAR19-NK cells acquired CD19 expression as well as other B cell-associated markers, such as CD20 and CD22, on their surface compared with NT-NK or 19scFv-NK controls (Fig. 1a,b and Extended Data Fig. 1a–d), suggesting that trogocytosis is a rapid process and that CAR signaling is necessary for the robust transfer of the cognate antigens to CAR-NK cells. A similar phenomenon, but to a lesser extent, was observed with CAR19-T cells (Supplementary Fig. 1a, as also previously described[8]). Pre-treatment of CAR-NK cells with Latrunculin A (LatA), an F-actin inhibitor that blocks immunologic synapse formation[24], prevented the transfer of cognate CD19 antigen from Raji cells to CAR19-NK cells (Fig. 1a,b), supporting the importance of synapse formation in driving trogocytosis. We therefore termed CAR-NK cells that acquired surface expression of target-derived cognate antigen following trogocytosis (Raji-derived CD19 in this case) as the TROG$^+$ fraction. TROG-antigen acquisition on CAR-NK cells coincided with a substantial reduction in CD19 expression on the targeted Raji cells, which could also be prevented by LatA pre-treatment of CAR-NK cells (Supplementary Fig. 1b,c). In contrast, CD19 was not selectively lost in coculture of Raji with NT-NK cells or 19scFv-NK cells (Fig. 1b and Supplementary Fig. 1c).

CAR19-NK cells also mediated strong trogocytic CD19 (tCD19) transfer after coculture with different CD19$^+$ targets such as NALM-6 cells, Ramos cells, healthy B cells and ovarian cancer cells that were genetically engineered to express CD19 (SKOV3^{gCD19+}; Supplementary Fig. 1d). Importantly, CAR19-mediated trogocytosis was also observed when CAR19-NK cells were cocultured with CD19$^+$ primary tumor cells derived from patients with either chronic lymphocytic leukemia (CLL) or acute lymphocytic leukemia (ALL), concurrent with a reciprocal reduction in CD19 on the targets (Fig. 1c and Supplementary Fig. 1e). To validate this observation with different cognate antigens, we synthesized CARs that recognized CD5, CD70, CD123, BCMA or ROR1, and evaluated their ability to mediate trogocytosis. A high level of cognate TROG-antigen was likewise detected on CAR-NK cells with the concurrent reduction of cognate antigen expression on cocultured targets (Supplementary Fig. 2a–e). Notably, CAR-mediated trogocytosis appeared to be antigen-specific since cognate antigen transfer above baseline (seen with NT-NK control) was not observed when the CAR molecule was mismatched with the target antigen and was influenced by the affinity of the CAR molecule for its targeted antigen (Supplementary Fig. 3a). Moreover, robust TROG-antigen transfer was not only observed with CD28/CD3ζ-based CAR signaling, but also with NK cells transduced with CARs signaling through CD3ζ only, DAP10$^{+/-}$ CD3ζ, NKG2D/CD3ζ, 41BB/CD3ζ and DAP12$^{+/-}$ CD3ζ (Supplementary Fig. 3b).

CAR-NK^{TROG+} cells are active but susceptible to fratricide. Trogocytosis has been reported to modulate NK cell function[15,17,18]. Thus, we next asked if TROG-antigen expression on CAR-NK cells could also modulate their effector function and whether this effect is positive or negative. We observed that soon after coculture with Raji targets, tCD19 was expressed on CAR19-NK cells (Extended Data Fig. 2a,b) and those CAR-NK^{TROG+} cells displayed significantly higher levels of degranulation (CD107a) and interferon-γ (IFN-γ) accumulation in response to Raji targets when compared with their TROG$^-$ counterparts (Fig. 1d), consistent with greater activation and effector potential[25]. To study this without the interference of using antibodies, we knocked out the endogenous *CD19* gene in Raji cells followed by transduction with a CD19–mCherry fusion molecule that could be easily detected upon transfer to CAR-NK cells through trogocytosis (Fig. 1e). We confirmed the rapid transfer of both CD19 and mCherry on CAR-NK cells upon engagement with Raji$^{CD19–mCherry}$ cells (Extended Data Fig. 2c–e). Notably, and in keeping with our previous findings, CAR-mediated CD19–mCherry transfer required the formation of an immunological synapse, since it was prevented by LatA pre-treatment (Fig. 1f); and it also depended on CAR activation as NK cells expressing 19scFv failed to transfer TROG-antigen to the same extent upon coculture with Raji$^{CD19–mCherry}$ cells (Fig. 1f). We also confirmed that fratricide was mediated by TROG-antigen recognition, since a significantly larger proportion of TROG$^+$ NK cell populations underwent apoptosis upon coculture with autologous CAR19-transduced NK cells compared with the control of 19scFv-NK^{TROG+} cells alone (Fig. 1g, Extended Data Fig. 3a–d and Supplementary Video 1). The addition of a CD19-blocking antibody to compete with CAR19 recognition and CD19 ligation reduced apoptosis of CAR19-NK^{TROG+} cells (Fig. 1g), indicating that the fratricide of the NK^{TROG+} population is mediated by on-target recognition, ligation and cytotoxic response by CAR-NK cells.

Antigen-mediated self-engagement drives NK cell exhaustion. Repeated antigenic stimulation by tumor cells is known to drive exhaustion of immune effector cells[26–28]. Indeed, we found that while expression of TROG-antigen was initially associated with higher CAR-NK cell activation, it did not result in sustained antitumor activity in a repeated tumor challenge model (Supplementary Fig. 4a–f). Thus, we asked if TROG$^+$ CAR-NK cells that did not succumb to fratricide are susceptible to functional exhaustion through repeated TROG-antigen-mediated CAR activation. CAR-NK cells were repeatedly challenged at a lower effector:target (E:T) ratio of 1:3 (to minimize fratricide) with either GFP-labeled Raji^{CD19+} cells or autologous NK cells that were genetically modified to stably express CD19 on their surface and GFP intracellularly (autoNK$^{gCD19+/GFP+}$ cells; Supplementary Fig. 4g). The level of CD19 expression on NK^{gCD19+} cells was approximately equivalent to that of tCD19 detected on CAR-NK^{TROG+} cells (Supplementary Fig. 4h,i). CAR19-NK cells cultured alone or after coculture with autoNK^{gGFP+} cells (lacking CD19 expression) were used as controls. In keeping with our rechallenge data with Raji tumor cells, CAR-NK effector cells (GFP-negative) that were repeatedly challenged with autoNK$^{gCD19+/GFP}$ cells acquired an exhaustion phenotype with a notable percentage (21 ± 9%) of cells co-expressing multiple checkpoints (PD1, TIM3 and TIGIT)[29,30], and a higher ratio of esomesodermin (EOMES) to T-bet[31–33] (Supplementary Fig. 4j). Further phenotypic interrogation using mass cytometry (cytometry by time-of-flight [CyTOF]) confirmed that over 65% of CAR-NK effector cells challenged with autoNK$^{gCD19+/GFP+}$ targets (clusters EC3–EC5; Fig. 2a,b) co-expressed PD1, TIGIT, LAG3 and TIM3 at different levels, with increased EOMES, and with downregulation of T-bet and Ki67, when compared with CAR-NK cells cultured alone or with autoNK^{gGFP+} cells that did not express CD19 (Fig. 2c). Acquisition of tCD19 from autoNK$^{gCD19+/GFP+}$ cells by CAR-NK effector cells (Extended Data Fig. 4a) was associated with downregulation of NK cell-activating receptors such as NKG2D, natural cytotoxicity receptors, CD16, 2B4 and adapter molecules (Syk, Zap70, DAP12 and SAP), as well as cytolytic proteins (granzymes and perforin; Fig. 2c). Interestingly, nearly 35% of CAR-NK cells (EC4–EC5) cocultured with autoNK$^{gCD19+/GFP+}$ also expressed higher levels of co-activating receptors such as NKG2C, DNAM-1, OX40 and CS1, as well as CD25 and CD69 (Fig. 2c), suggesting that CAR-NK cells only acquire their exhausted phenotype after CAR-antigen-mediated self-engagement and activation.

Based on our phenotypic observation, we hypothesized that repeated antigenic challenge by sibling autoNK$^{gCD19+/GFP+}$ cells drives the functional exhaustion of CAR-NK cells. To test this, we isolated CAR-NK effector cells (GFP-negative) after 4 d of coculture with autoNK$^{gCD19+/GFP+}$ cells (GFP-positive), and compared

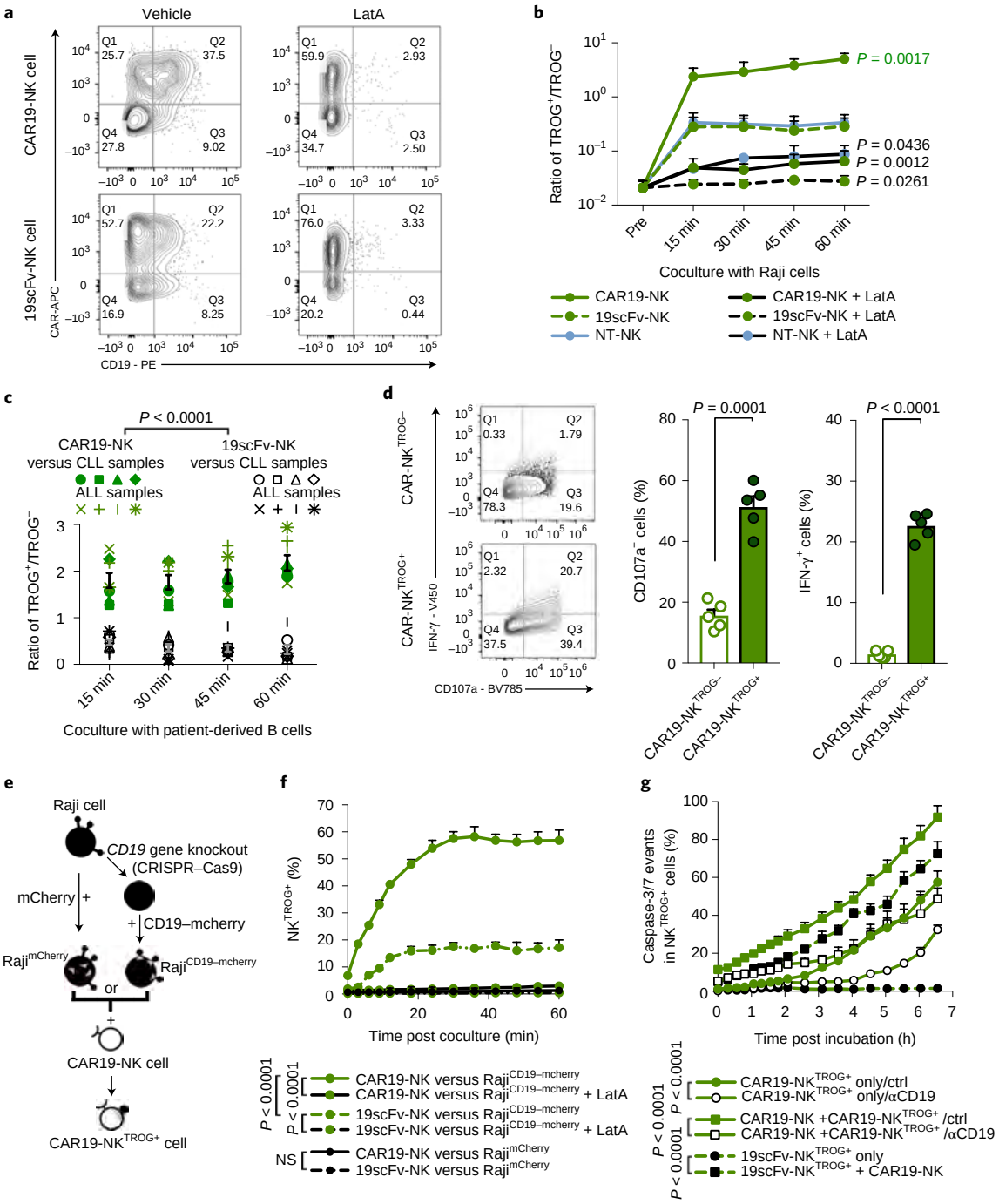

Fig. 1 | CAR19-mediated trogocytosis in NK cells cocultured with CD19⁺ tumor targets. a, FACS plots show CD19 expression on NK cells transduced with CAR19 or 19scFv (no intracellular signaling domain) after coculture with Raji cells for 5 min with LatA or vehicle control (representative for 3 donors). The CD19⁺ gate was determined based on fluorescence minus one (FMO) control and by referring to NK cells cultured alone. **b**, tCD19 (shown as the ratio of TROG⁺/TROG⁻) expression on singlet CAR19-NK, 19scFv-NK and NT-NK cells after coculture with Raji cells ($n = 3$ donors). TROG⁺ fractions comprised NK cells expressing CAR⁺CD19⁺ (for example, Q2 from **a**), while the TROG⁻ fractions included NK cells expressing CAR⁺CD19⁻ (for example, Q1 from **a**). **c**, tCD19 expression (shown as the ratio of TROG⁺/TROG⁻) on singlet CAR19-NK (green symbols) or 19scFv-NK cells (black symbols) after coculture with B-CLL cells ($n = 4$ patients) or B-ALL cells ($n = 4$ patients). **d**, Expression of CD107a and IFN-γ in TROG⁺ versus TROG⁻ CAR19-NK cells 6 h after stimulation with Raji cells (representative of 3 donors). Bar graphs show the percentages of CD107a⁺ and IFN-γ⁺ cells in each fraction normalized to expression in CAR19-NK cells cultured alone ($n = 5$ donors). **e**, Strategy for CD19–mCherry fusion protein expression on *CD19*-knockout Raji (Raji$^{CD19\text{-}KO}$) cells, controlled by Raji cells genetically modified for intracellular mCherry expression (Raji^{mCherry}). **f**, Percentage of CAR19-NK cells or 19scFv-NK cells expressing mCherry after coculture with Raji$^{CD19\text{–}mCherry}$ cells or Raji^{mCherry} in different conditions in an Incucyte assay (representative of 3 donors). **g**, Incucyte analyses showing the percentage of caspase-3/7 events in the TROG⁺ fraction of CAR19-NK cells versus 19scFv-NK cells cultured alone, or with autologous fresh CAR19-NK cells. For CAR19-NK^{TROG+} cells, anti-human CD19-blocking antibody (αCD19) or an antigen-mismatched scFv antibody were added as controls (representative of 3 donors). *P* values were determined by two-tailed two-way ANOVA in **b**, **c**, **f** and **g**, or by two-sided Student's paired *t*-test in **d**; NS, not significant. Data were shown by mean + s.e.m. Inset numbers indicate percentages in respective quadrants. Each circle represents an individual donor or experimental replicate.

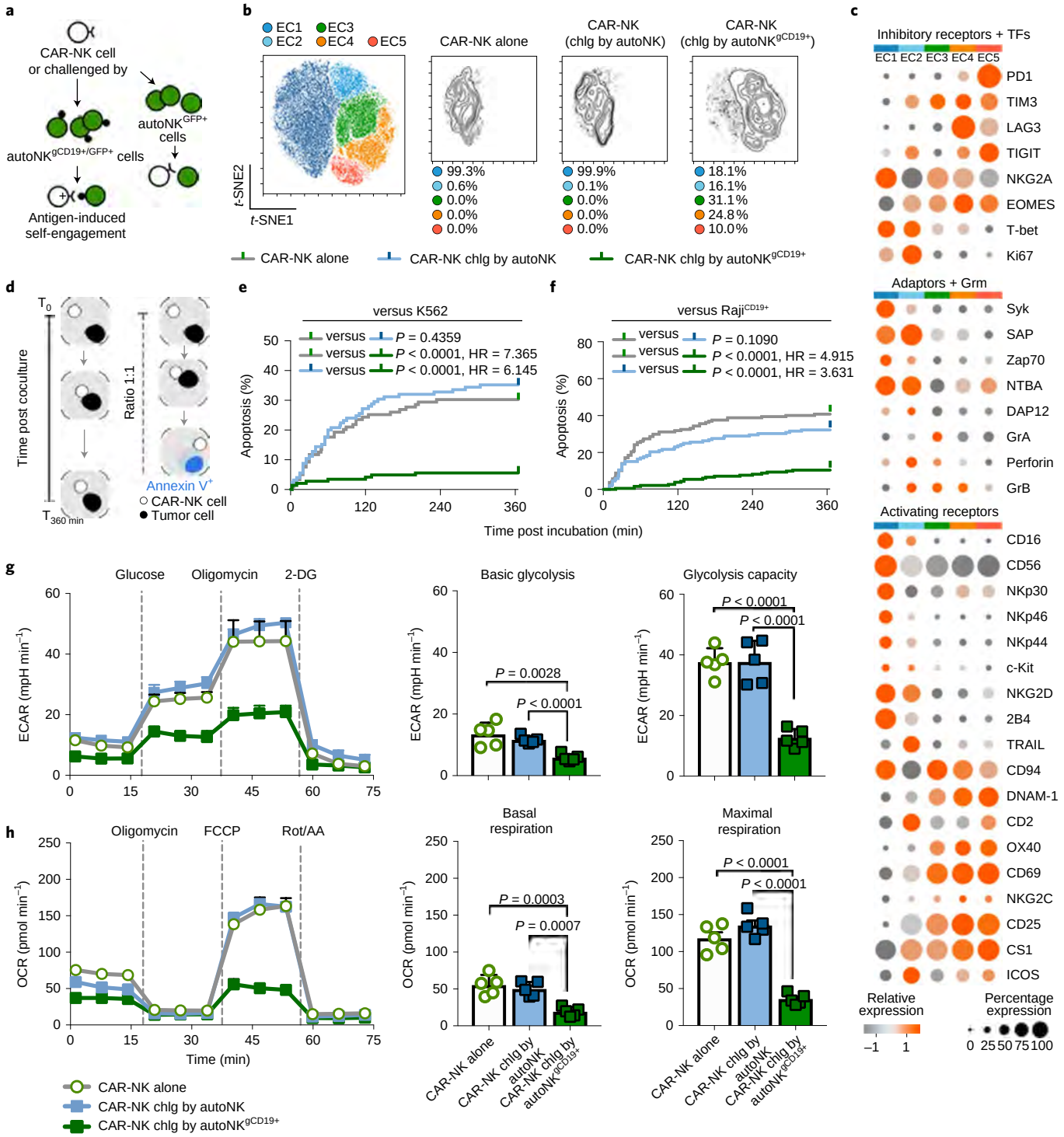

their cytotoxicity with that of CAR-NK cells cultured alone or cocultured with autoNK^{GFP+} cells. In each Nanowell, only one CAR-NK effector cell was incubated with its target cell to rule out the possibility of fratricide (Methods and Fig. 2d). At the single-cell level, CAR19-NK cells that were continuously activated through fratricide (versus autoNK$^{gCD19+/GFP+}$) killed significantly fewer K562 targets (Fig. 2e and Supplementary Video 2) and CD19^{+} Raji tumor targets (Fig. 2f, Extended Data Fig. 4b,c and Supplementary Video 3) when compared with controls, and this was especially the case at lower E:T ratios and after multiple rounds of rechallenge with autoNK$^{gCD19+/GFP+}$ cells (Extended Data Fig. 4d–f). Together, these findings confirm impaired CAR-NK effector function resulting from antigen-induced self-engagement.

Given the importance of cellular metabolic fitness for NK cell effector function[34,35], we also evaluated whether CAR-NK cells cocultured with autoNK$^{gCD19+/GFP+}$ had dysregulated metabolic capacity. Compared with controls, CAR-NK cells previously challenged with autoNK$^{gCD19+/GFP+}$ had notable impairment in their metabolic machinery at their baseline level (without stimulation) and in response to the maximum stimulation, with a substantial reduction in their glycolytic capacity as measured by the extracellular acidification rate (ECAR; Fig. 2g), and oxygen consumption rate (OCR) and oxidative phosphorylation (OXPHOS; Fig. 2h). Taken together,

Fig. 2 | Impact of antigen-induced self-engagement on CAR-NK effector cell phenotype and function. a, Schematic illustrating a rechallenge (chlg) assay using autoNK^{gCD19+} at an E:T ratio of 1:3, controlled by coculture with autoNK cell (lacking CD19 expression). Both autoNK^{gCD19+} and autoNK cells were genetically modified to express intracellular GFP to facilitate their identification. **b**, *t*-SNE analysis of live NK$^{CAR19+/GFP-}$ cells after the second round of rechallenge with autoNK$^{gCD19+/gGFP+}$ cells; controls include CAR19-NK cells alone or after 4 d of coculture with autoNK^{gGFP+} cells (no CD19 expression). Cells were evaluated by CyTOF, and merged to create a single *t*-SNE map (10,000 cells from 3 pooled donors per condition). Each cluster (EC1–EC5) is represented in a different color, and frequencies are indicated for each culture condition. **c**, Heatmap for expression of key NK cell phenotypic and functional markers. Expression of each marker is represented by colors gray (low) to orange (high) and the size of the circle. TFs, transcription factors; Grm, granzyme. **d**, Schematic illustrating single-cell time-lapse imaging cytotoxicity assay. Time was recorded over 6 h (T_0–$T_{360\ min}$) for a single CAR-NK cell cocultured with a single tumor cell. During the incubation, Annexin V influx in the tumor cell was determined as a marker of apoptosis. **e**,**f**, Kaplan–Meier curves showing the percentage of apoptosis in targeted cells when CAR-NK cells were cocultured with K562 cells (**e**) or Raji cells (**f**) (gray, CAR-NK cells alone; blue, CAR-NK cells isolated after 4 d of coculture with autoNK$^{CD19-/GFP+}$ cells; green, CAR-NK cells isolated after the second round of rechallenge by autoNK$^{gCD19+/GFP+}$ cells). **g**, Ex vivo analysis of CAR-NK cell glycolytic fitness by ECAR; bar graphs showing their basal ECAR (left; $n=5$ donors), and their maximum ECAR (right; $n=5$ donors). **h**, Oxidative phosphorylation (OXPHOS) of CAR-NK cells by OCR; bar graphs showing their basal OCR (left; $n=5$ donors), and their maximal OCR (right; $n=5$ donors). *P* values were determined by log-rank test in **e** and **f**, or by two-sided Student's *t*-test in **g** and **h**. Data were shown by mean + s.e.m. Each symbol represents an individual donor-derived CAR-NK cell sample. FCCP, carbonyl cyanide 4-(trifluoromethoxy)phenylhydrazone; HR, hazard ratio; Rot/AA, Rotenone and antimycin A.

these data support a model in which continuous CAR activation, via self-engagement with the TROG-antigen, drives the functional exhaustion and metabolic dysregulation of CAR-NK cells.

TROG-antigen expression reduces CAR-NK cell persistence. To investigate the in vivo kinetics of TROG-antigen acquisition by CAR-NK cells, we xenografted mice with three escalating dose levels of Raji cells (0.2×10^5, 1×10^5 or 0.5×10^6), respectively, to cover the various levels of tumor burden, followed by a single infusion of CAR-NK cells (Methods and Extended Data Fig. 5a,b). In keeping with our in vitro data, substantial fractions of CD19-expressing CAR19-NK cells (CAR19-NK^{tCD19+}) were detected as early as 6 days post-infusion, with the TROG$^+$ population increasing over the treatment course, regardless of their initial tumor burden (Extended Data Fig. 5c). The transfer of tCD19 to CAR-NK cells was also associated with a decrease in CD19 expression on Raji cells (Extended Data Fig. 5d), but the same phenomenon was not observed in mice treated with ex vivo-expanded NT-NK cells (Extended Data Fig. 5e), suggesting a robust in vivo CAR-mediated trogocytosis. Notably, CD19 expression in Raji cells collected from the organs of the animals returned to baseline after a short-term period of ex vivo culture (Supplementary Fig. 5a), with the restoration of their susceptibility to CAR-NK cell-mediated cytotoxicity in vitro (Supplementary Fig. 5b). Notably, in vivo acquisition of TROG-antigen by CAR-NK cells was associated with a reduction in their cell number and lower viability when compared with controls (Extended Data Fig. 6a–e), suggesting that trogocytosis of the CD19 antigen was associated with fratricide that contributed to the substantial in vivo loss of CAR19-NK cells.

Similar observations were detected in mouse models treated with anti-CD5 CAR-NK cells (grafted with CCRF^{CD5+}; Supplementary Fig. 6a–e) and anti-CD123 CAR-NK cells (grafted with MOLM-14^{CD123+}; Supplementary Fig. 7a–e). Together, our findings suggest that TROG-antigen-induced in vivo fratricide of CAR-NK cells was quite common, if not universal.

CAR-NK^{TROG+} cells accumulate during tumor progression in vivo. We next used a noncurative mouse model of Raji tumor, where a single dose of CAR-NK cell infusion could initially control tumor progression, but was frequently followed by tumor relapse[36,37]. Mice were killed at regular intervals following CAR-NK cell infusion, with their blood and tissues collected for comprehensive phenotypic analysis by CyTOF (Extended Data Fig. 7a,b). Using a *t*-distributed stochastic neighbor embedding (*t*-SNE) map, we observed four major clusters of CAR-NK cells (Fig. 3a). Pre-infusion CAR-NK cells were exclusively clustered in C1 (more than 99%; Fig. 3b), but cells from early time points post-infusion were predominantly found in C2 (more than 66%; Fig. 3b); at later time points and during the relapse phase, the majority of CAR-NK cells were segregated in C3 and C4 (73–97%; Fig. 3b), with higher expression of TROG-antigen (such as tCD19) when compared with their non-CAR-expressing NK counterparts (Fig. 3c). In vivo acquisition of TROG-antigen was associated with higher expression of both activation and inhibitory markers (Extended Data Fig. 7c,d). Notably, CAR-NK cells in C3 and C4 showed higher expression of checkpoint markers (PD1, TIM3, TIGIT); lower expression of transcription factors, cytolytic proteins and adapter molecules; but upregulation of cytokine receptors interleukin-2 (IL-2) receptor (IL-2R) (CD25), SCF receptor (c-Kit), co-activating receptors (NKG2C, 2B4, DNAM-1) and

Fig. 3 | Impact of TROG-antigen acquisition on CAR-NK cell phenotype and function in vivo. a, *t*-SNE analysis of live hCD45$^+$GFP$^-$CD56$^+$CD3$^-$ NK cells collected from different organs (blood, bone marrow, spleen and liver) of mice at different points during the treatment course. Phenotypic signatures of all collected NK cells were evaluated by mass cytometry and merged to create a single *t*-SNE map. **b**, Contour plots showing the *t*-SNE cluster prevalence in the pre-infusion product, 2 weeks after infusion, 3–4 weeks after infusion or at the endpoint. The number of cell objects for each condition was indicated. **c**, Frequencies of NK cells expressing the TROG-antigen (tCD19) in the CAR19-positive (green) or CAR-negative (blue) fractions at different time points during treatment are presented, controlled by their counterparts in the pre-infusion product. **d**, Heatmap representing the expression levels of phenotypic and functional markers on CAR-NK cells within each cluster. The expression level for each marker is represented by the colors gray (low) to orange (high) and the size of the circle. **e**, FlowSOM analysis of post-infusion NK cell populations where each metacluster is mapped using a self-organizing mapping strategy. Each colored region corresponds to a metacluster with inserted pie chart representing the frequency of NK cells expressing CAR and TROG-antigen (tCD19) on clustered cells; the size of each chart represents the number of clustered cells. **f**,**g**, Violin plots showing the expression of CAR19 (**f**) and tCD19 (**g**) on CAR19-NK cells in each cluster, determined based on their level in pre-infused NT-NK cells shown as the gray line. **h**, Violin plot showing cisplatin levels in post-infusion CAR19-NK^{TROG+} cells (expressing CD19) or their CAR19-NK^{TROG-} counterparts for each cluster. Cisplatin level represents the cellular viability of each population. **i**–**l**, Violin plots showing the expression of c-Kit, EOMES and T-bet (**i**); Zap70, Syk and 2B4 (**j**); Granzyme (Gr) A, GrB and perforin (**k**); and PD1, TIM3 and TIGIT (**l**) in TROG$^+$ and TROG$^-$ fractions of CAR19-NK cells. The median expression strength for each marker in CAR19-NK cells before infusion (in C1) is indicated by the gray line. *P* values were determined by two-tailed Wilcoxon matched pairs test.

chemokine receptors (Fig. 3d), which is consistent with a previously activated phenotype and eventual exhaustion[27,38,39].

We next remapped cells to metaclusters using FlowSOM, an unbiased gating method from the inbuilt algorithm of *t*-SNE[40], to compare the phenotypic signatures of TROG$^+$ versus TROG$^-$ CAR-NK cells (Fig. 3e). Indeed, in keeping with our earlier results, expression of tCD19 on CAR-NK cells was associated with a reduction in their in vivo viability, as shown by the accumulation of cisplatin (Fig. 3f–h and Extended Data Fig. 7e). However, this phenomenon was not observed in NK^{TROG+} cells from mice treated with NT-NK cells alone (Extended Data Fig. 7f), confirming our in vitro results that NK cell fratricide was antigen-specific and depended upon recognition and ligation of CAR with the TROG-antigen. In addition, when compared with the TROG$^-$ CAR-NK cell population, TROG$^+$ CAR-NK cells displayed higher expression of c-kit, T-bet, EOMES, activating adapters and cytolytic proteins (Fig. 3i–k), while also expressing checkpoint markers such as TIGIT, PD1 and TIM3 (Fig. 3l), especially at late time points (exclusively in C4). These data suggest that acquisition of TROG-antigen on CAR-NK cells was associated with activation first, followed by fratricide, functional exhaustion and failure of NK cells to control the tumor in vivo.

At the messenger RNA level, B cell markers (*CD19*, *MSA41*) were not detected in the NK cell clusters (defined by *NKG7* and *FCGR3A* expression; Extended Data Fig. 7g). Taken together, these findings

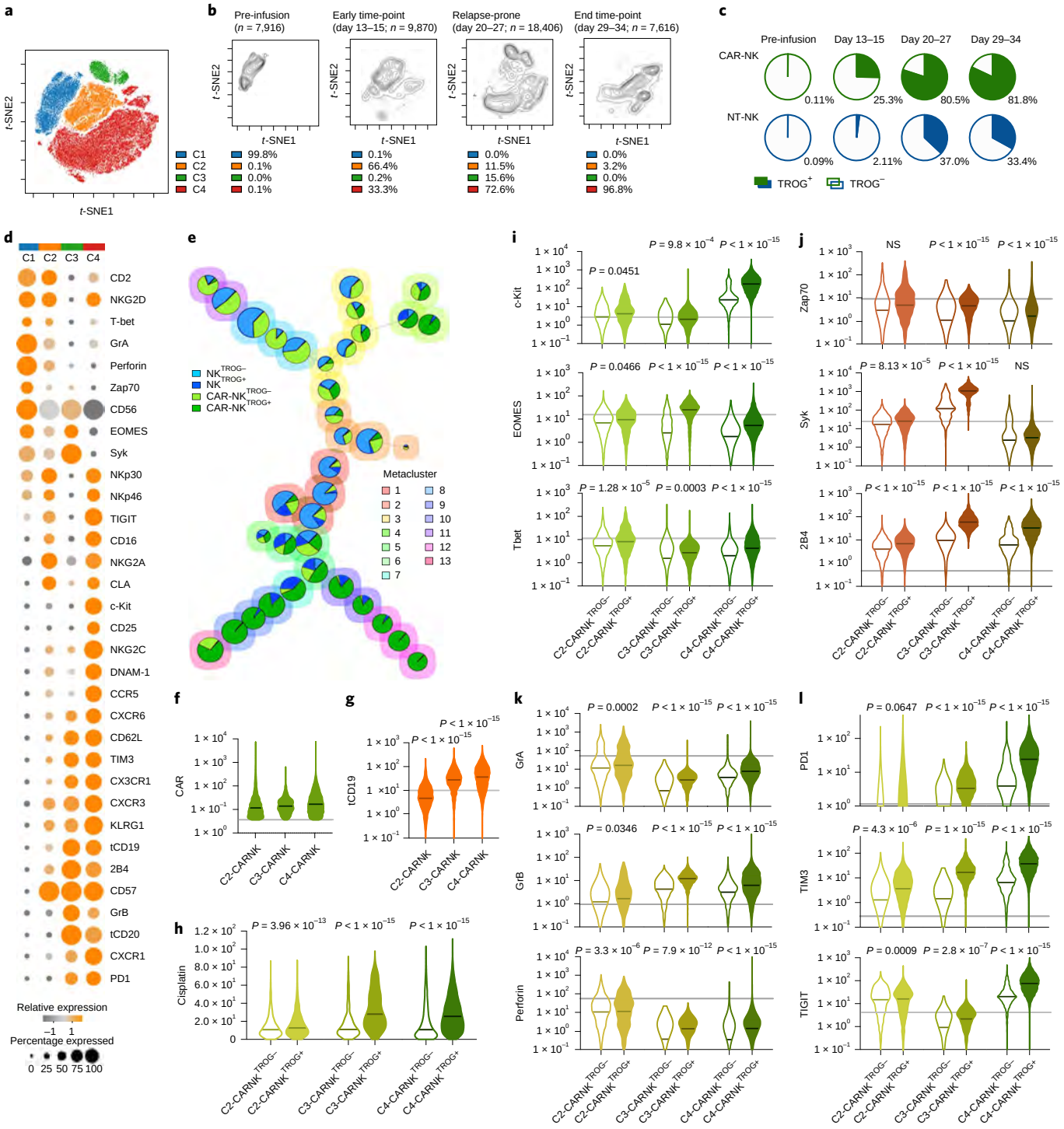

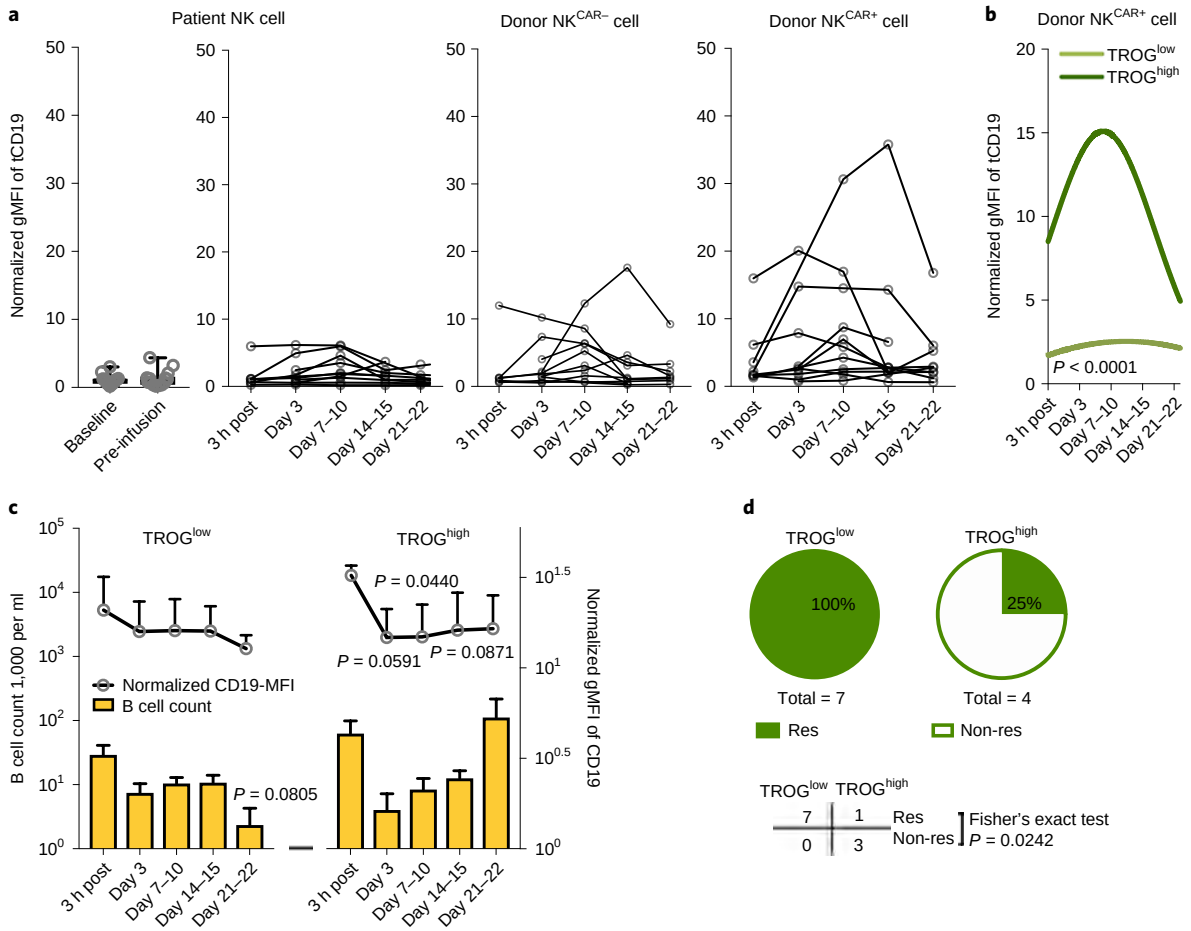

Fig. 4 | A lower level of CAR-mediated TROG-antigen expression was associated with improved clinical response to CAR-NK cell-based immunotherapy. **a**, tCD19 expression on singlet cells of patient-derived NK cells, donor-derived non-CAR-expressing NK cells (NK^{CAR-}), and donor-derived CAR-expressing NK cells (NK^{CAR+}) at different time points after receiving CAR19-NK cell immunotherapy. gMFI of tCD19 expression was assessed by flow cytometry. Samples from individual patients at different times after CAR-NK cell infusion are presented. **b**, Nonlinear regression analyses using polynomial models show tCD19 expression on donor-derived NK^{CAR+} cells over time after CAR-NK cell infusion. The normalized mean tCD19 gMFI on CAR19-NK cells for the whole patient population was 6.29 (range of 0.61–35.77). Patients with a high (>mean) versus low (≤mean) normalized tCD19 gMFI at more than one time point were defined as group of $TROG^{high}$ ($n=4$ patients) versus $TROG^{low}$ ($n=7$ patients), respectively. **c**, CD19 expression (upper) and cell counts (lower) for singlet $CD19^+$ B cells in the $TROG^{low}$ versus $TROG^{high}$ patient groups at different time points after CAR-NK cell infusion. **d**, Pie charts showing the number of responders (Res, left) versus nonresponders (Non-res, right) after receiving CAR19-NK cell infusion in the $TROG^{low}$ versus $TROG^{high}$ groups. *P* value was determined by two-tailed two-way ANOVA in **b**, two-sided Student's *t*-test in **c**, two-tailed Fisher's exact test in **d**; data were assessed by mass cytometry and shown as mean + s.e.m. Each circle represents an individual patient.

confirm that TROG-antigen expression on CAR-NK cells is mediated by post-transcriptional transfer of protein from tumor targets which leads to activation, fratricide and eventual exhaustion of infused CAR-NK cells.

Lower TROG-antigen expression favors clinical response. We next investigated if trogocytosis contributes to CAR-NK cell fratricide and tumor progression in patients with lymphoid malignancies treated in our previously reported CAR-NK cell trial (NCT03056339)[41]. Using peripheral blood samples collected at multiple time points after CAR-NK cell infusion, patients were divided into two groups based on the overall tCD19 expression in CAR-NK cells ($TROG^{high}$ ($n=4$) versus $TROG^{low}$ ($n=7$); Fig. 4a,b and Supplementary Fig. 8). Acquisition of tCD19 expression on CAR-NK cells was associated with a reciprocal reduction in CD19 expression on B cells and a higher probability of relapse (3 of 4 patients) compared with patients in the $TROG^{low}$ group (0 of 7 patients; Fig. 4c,d). Although this analysis was based on a small number of patients, our clinical observations further support the unfavorable effect of CAR-mediated trogocytosis on the antitumor efficacy of CAR-NK cells.

iCAR against an NK-antigen prevents self-engagement by aCAR. The dynamic balance of activating and inhibitory signals determines NK cell-mediated cytotoxicity and target lysis[22,23]. Thus, we used a genetic engineering strategy that exploits the physiological HLA class I-mediated NK cell inhibition to control NK cell activity in an antigen-specific manner[20–22]. We hypothesized that an iCAR, which incorporated an scFv directed to an NK-specific antigen linked to a powerful NK cell inhibitory signal, could limit NK cell responsiveness despite the simultaneous antigen engagement of an aCAR, thus allowing for on-target/on-tumor recognition.

We designed a series of iCAR constructs that fused an antigen-specific scFv with the transmembrane domain and immunoreceptor tyrosine-based inhibition motifs (ITIMs) derived from key NK cell inhibitory receptors (KIR2DL1 (ref. [42]), LIR-1 (ref. [43]), CD300A (ref. [44]), NKG2A (ref. [45]) and LAIR-1 (ref. [46])). As proof of principle, we first tested an scFv specific for CD19 and confirmed

that anti-CD19 iCARs (iCAR19s) were expressed on the surface of NK cells at similar levels to their aCAR-NK cell counterparts (CAR19: CD28/CD3ζ-based; Extended Data Fig. 8a,b). We next asked if iCARs limit NK cell activity in an antigen-specific manner by culturing iCAR19-expressing NK cells with CD19$^+$ targets and measuring the phosphorylation status of inhibitory signals versus activating signals upon target engagement[22,47,48]. Antigen stimulation resulted in higher phosphorylation of SHP1 in iCAR19-expressing NK cells (Extended Data Fig. 8c), without inducing phosphorylation in immunoreceptor tyrosine-based activation motif (ITAM) adapter proteins (Sky and Zap70; Extended Data Fig. 8d). Additionally, iCAR19-NK cells produced fewer effector cytokines with lower cytotoxicity against CD19$^+$ targets (such as Raji cells, or autoNK^{gCD19+} cells), but not against CD19-negative targets such as K562 or CD19-KO Raji cells (Extended Data Fig. 8e–j). Of note, iCARs did not negatively impact the proliferation of NK cells cultured with an engineered K562 cell line (universal antigen presenting cells [uAPCs]) and IL-2 (Extended Data Fig. 8k,l). Compared with the CD19-aCARs, trogocytosis was significantly less with iCARs, with the lowest level observed when NK cells were transduced with an iCAR incorporating a KIR2DL1 (iCAR1; Extended Data Fig. 8m). Thus, for all subsequent experiments, the signaling endodomain for KIR2DL1 (iCAR1) was used.

To determine if iCARs can inhibit the on-target off-tumor fratricide mediated through the aCAR, we next sought to synthesize an iCAR that recognized an NK self-antigen by fusing the transmembrane and intracellular domains of iCAR1 with an scFv targeting CS1, a co-receptor that is constitutively expressed on all normal NK cells[49,50], but absent on most CD19$^+$ lymphoid-derived malignancies[51,52](Supplementary Fig. 9a,b). We confirmed that CS1 was expressed at high levels on NK^{TROG+} cells both in vitro and in vivo (Supplementary Fig. 9c–f). Primary NK cells were transduced with the AI-CAR system (aCAR targeting CD19: aCAR19; and iCAR targeting CS1: iCAR1-CS1), and evaluated for their function against different targets (Fig. 5a,b). Controls included 19scFv and CS1scFv without activating or inhibitory signaling endodomains, respectively. iCAR-CS1 expression spared the on-target antitumor activity of aCAR19 against CD19$^+$ tumor targets (Fig. 5c), including primary CLL samples from patients (Fig. 5d and Supplementary Fig. 10a), but inhibited the activity of aCAR-NK cells when both CD19 and CS1 were expressed on the target (Fig. 5e and Supplementary Fig. 10b). We next investigated the ability of iCAR to restrict aCAR-mediated cytotoxicity against autoNK-$^{gCD19+/CS1+}$ cells. NK cells expressing the AI-CARs displayed marked reduction in cytotoxicity and fratricide against autoNK$^{gCD19+/CS1+}$ cells (Fig. 5f), but maintained their effector function and cytokine response to CD19$^+$CS1$^-$ target cells (Supplementary Fig. 10c,d), with no evidence of exhaustion (Fig. 5g,h) or significant impairment in their in vitro proliferation capacity (Fig. 5i). Notably, iCAR expression had little impact on aCAR-mediated cognate-antigen trogocytosis in cocultures of NK cells with CD19$^+$CS1$^-$ Raji targets (Fig. 5j). These findings confirmed that the CS1-targeting iCAR selectively prevents NK cells from antigen-induced on-tumor/off-target effect, while preserving the therapeutic response of the aCAR against 'on-target' CD19$^+$ tumor cells.

AI-CARs improve in vivo antitumor activity of NK cells. To investigate whether AI-CAR-NK cells could protect NK cells from aCAR-mediated fratricide and exhaustion in vivo, we used our well-established NSG mouse model with Raji tumor[36,37]. Mice received one dose of 1×10^7 NK cells expressing anti-CD19 aCAR/anti-CS1 iCAR1, with controls of NK cells expressing anti-CD19 scFv/anti-CS1scFv, anti-CD19 scFv/anti-CS1 iCAR1 or anti-CD19 aCAR/anti-CS1scFv (Fig. 6a). The anti-CD19 aCAR/anti-CS1 iCAR1-NK cells mediated the strongest antitumor response, with a significantly lower bioluminescence imaging (BLI) signal and better overall survival compared with the control groups (Fig. 6b–d). To confirm that the improved in vivo antitumor response is mediated through a decrease in TROG-antigen-induced fratricide and improved effector function by AI-CAR-NK cells, in a parallel experiment we killed mice at serial time points and collected blood and organs for NK cell profiling. While the AI-CAR-NK cells did not impact the extent of aCAR-mediated trogocytosis (Fig. 6e), we observed less trogocytosis-mediated in vivo fratricide, as evidenced by the better viability, higher persistence (Fig. 6f–h and Supplementary Fig. 11a–e) and improved effector function compared with the control groups (Fig. 6i and Supplementary Fig. 11f).

We also investigated the validity of our results in a solid tumor model of ovarian cancer. We intraperitoneally injected SKOV3 cells that were endogenously expressing ROR1, or genetically engineered to express CD19 (SKOV3^{gCD19+}), into NSG mice, followed by a single infusion of NK cells co-expressing antigen-specific AI-CARs or the relevant scFv controls (Fig. 6j and Extended Data Fig. 9a). Again, we observed superior antitumor control with AI-CAR-NK cells (Fig. 6k–m and Extended Data Fig. 9b–d), associated with improved NK cell viability, persistence and infiltration within the tumor microenvironment with variable expression of the ROR1 TROG-antigen on their surface (Fig. 6n–q and Extended Data Fig. 9e–i). Taken together, these results provide evidence that iCARs limit the aCAR response to the TROG-antigen on NK cells in an antigen-specific fashion in vivo, reducing fratricide and preserving NK cell effector function and persistence without abrogating the aCAR response to the tumor target, and thus resulting in improved NK cell antitumor activity.

Discussion

Trogocytosis is a well-described phenomenon by which lymphocytes extract plasma membrane fragments from their targets following immunological synapse formation[1,2,4]. In this study, we revealed a unique mechanism for tumor escape following CAR-NK cell therapy, specifically that activation of aCAR drives the transfer of target antigen from tumor cells that are engaged but not killed by NK cells. The aCAR-NK cells that acquired TROG-antigen, in turn, become target cells (antigen-induced self-recognition) and are lysed by other aCAR-NK cells while those that are not killed by fratricide become hyporesponsive, similar to reports with CAR-T cells[8,53]. This phenomenon is associated with a concurrent loss of target antigen on the cancer cells, rendering them less susceptible to aCAR-mediated killing, and, thus, increasing the risk of tumor relapses. Finally, we showed that a dual AI-CAR system that combines an extracellular domain targeting an NK-specific antigen with the signaling endodomain from an inhibitory KIR (iCAR) successfully achieves antigen-specific suppression of aCAR-mediated NK cell fratricide and hyporesponsiveness, while retaining their on-target antitumor activity with improved persistence in multiple in vivo models (Extended Data Fig. 10a,b).

Intercellular protein transfer is mediated through multiple pathways[2,54,55]. Among these, trogocytosis is a well-described phenomenon that mediates surface protein transfer from targets to NK cells[5,56,57], and has been shown to substantially impact NK cell function[15,17,18]. For instance, NKG2D-mediated trogocytosis of NKG2D-ligands has been associated with NK cell hyporesponsiveness and fratricide[15,16,19,58]. Similarly, trogocytosis triggered by the engagement of the CD16 receptor on NK cells with monoclonal antibodies leads to target antigenic modulation and compromised therapeutic efficacy[59,60]. A recent study reported how trogocytosis promotes antigen density reduction and T cell exhaustion and fratricide after CAR-T cell therapy[8]. To our knowledge, our study is the first to show that human CAR-NK cells acquire cognate-antigen targets from tumor cells through antigen-specific trogocytosis that requires CAR activation and signaling. This phenomenon was observed with CARs expressing different CAR-signaling endodomains and targeting different antigens, but the degree of trogocytosis was

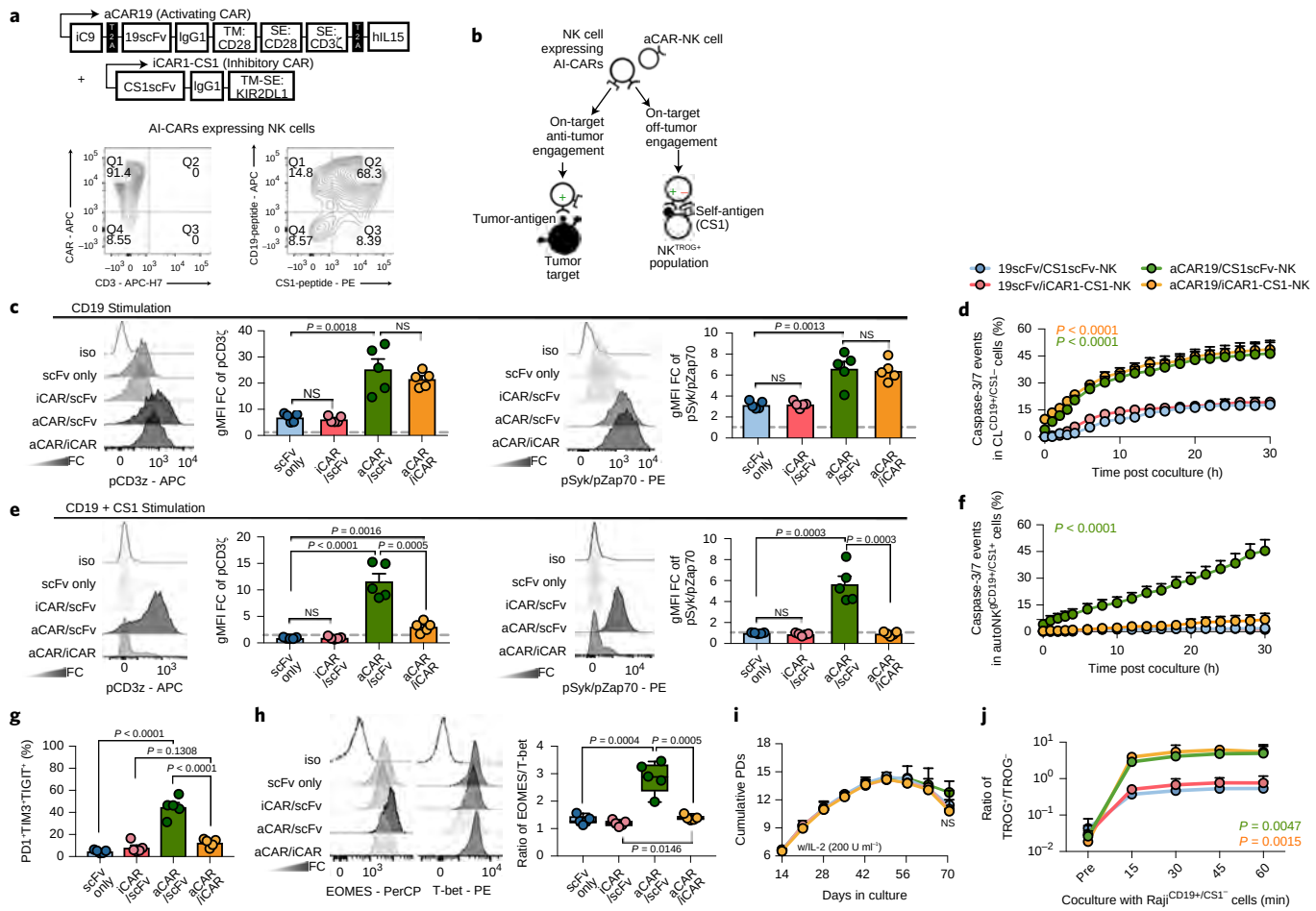

Fig. 5 | Expression of an iCAR by NK cells reduced fratricide and exhaustion induced by aCAR. a, Schematic of the retrovirus vector for aCAR19 and iCAR1-CS1. Flow cytometric analysis shows dual expression of aCAR19 and iCAR1-CS1 on NK cells, measured by tagged peptides (CD19 and CS1). TM, transmembrane; SE, signaling endodomain. CAR expression levels are indicated within respective quadrants. **b**, Diagram illustrating engagement of AI-CAR-expressing NK cells with their targets; red symbol indicates inhibitory signal '−', green symbol indicates activating signal '+'. **c**, Phos-CD3ζ (pCD3z, left) and phos-Syk/Zap70 (right) levels in NK cells expressing 19scFv/CS1scFv (scFv only, no intracellular signaling; blue), 19scFv/iCAR1-CS1 (iCAR/scFv; red), aCAR19/CS1scFv (aCAR/scFv; green) or aCAR19/iCAR1-CS1 (aCAR/iCAR; yellow) after stimulation with Raji$^{CD19+/CS1-}$ cells; the following bar graphs show fold change (FC) in gMFI after normalization to isotype control ($n=5$ donors per condition). **d**, Incucyte analyses showing caspase-3/7 events in CD19$^+$CS1$^-$ primary CLL cells after coculture with CAR-NK cells, controlled by scFv-expressing NK cells ($n=3$ donors per condition). **e**, Phos-CD3ζ (pCD3z, left) and phos-Syk/Zap70 (right) levels in NK cells expressing 19scFv/CS1scFv, 19scFv/iCAR1-CS1, aCAR19/CS1scFv or aCAR19/iCAR1-CS1 stimulated with CD19$^+$ autoNK^{CS1+} cells; bar graphs show the FC in gMFI after normalization to isotype control ($n=5$ donors per condition). **f**, Incucyte analysis showing caspase-3/7 events in gCD19$^+$CS1$^+$ autoNK cells after coculture with CAR-expressing NK cells, controlled by scFv-expressing NK cells ($n=3$ donors per condition). **g**,**h**, Co-expression of PD1, TIM3 and TIGIT (**g**), and ratio of EOMES/T-bet (**h**) in singlet CAR-NK cells after the second round of antigen challenge with autoNK$^{gCD19+/CS1+/GFP+}$ cells ($n=5$ donors). Representative flow histograms for EOMES and T-bet were shown. **i**, Cumulative population doublings (PDs) for each CAR-expressing NK cell condition ($n=3$ donors) over 70 d of culture with IL-2. **j**, tCD19 expression (shown as ratio of TROG$^+$/TROG$^-$) on singlet CAR-expressing NK cells ($n=3$ donors) after coculture with Raji cells, controlled by scFv-expressing NK cells (representative of 3 donors). *P* values were determined by two-tailed two-way ANOVA in **d**, **f**, **i** and **j**, or by two-sided Student's *t*-test in **c**, **e**, **g** and **h**. Data were assessed by flow cytometry in **a**, **c**, **e**, **g**, **h** and **j**, and are shown as mean + s.e.m, or medium (min/max) in boxplots. Each circle represents an individual donor.

influenced by the density of the antigen on tumor cells as well as the affinity of the CAR for its cognate ligand. Interestingly, however, high binding-affinity scFv domain did not always result in a high level of TROG-antigen transfer, possibly because other factors could also play a role such as rate of disassociation from the cognate antigen. Given that TROG-antigen-expressing NK cells are susceptible to aCAR-NK cell cytotoxicity by induced self-recognition, preventing trogocytosis could be a beneficial approach to improving the efficacy and in vivo persistence of aCAR-NK cells.

However, to date, there are no strategies that can be applied therapeutically to regulate trogocytosis in a specific manner. Here, we developed an engineering approach that took advantage of normal NK cell biology and employed an ITIM-containing iCAR to suppress the aCAR-mediated recognition of TROG-antigen-expressing NK cells (on-target/off-tumor recognition of TROG$^+$ NK cells), while retaining the aCAR activity against tumor targets. By combining the activity of two chimeric receptors, one of which generated a dominant negative signal upon recognition of an NK-specific antigen and one that induced an activating signal upon engagement with the tumor target, we could successfully switch off the response of the counteracting aCAR activation against the TROG-antigen on NK cells in an antigen-specific manner, while sparing their activity

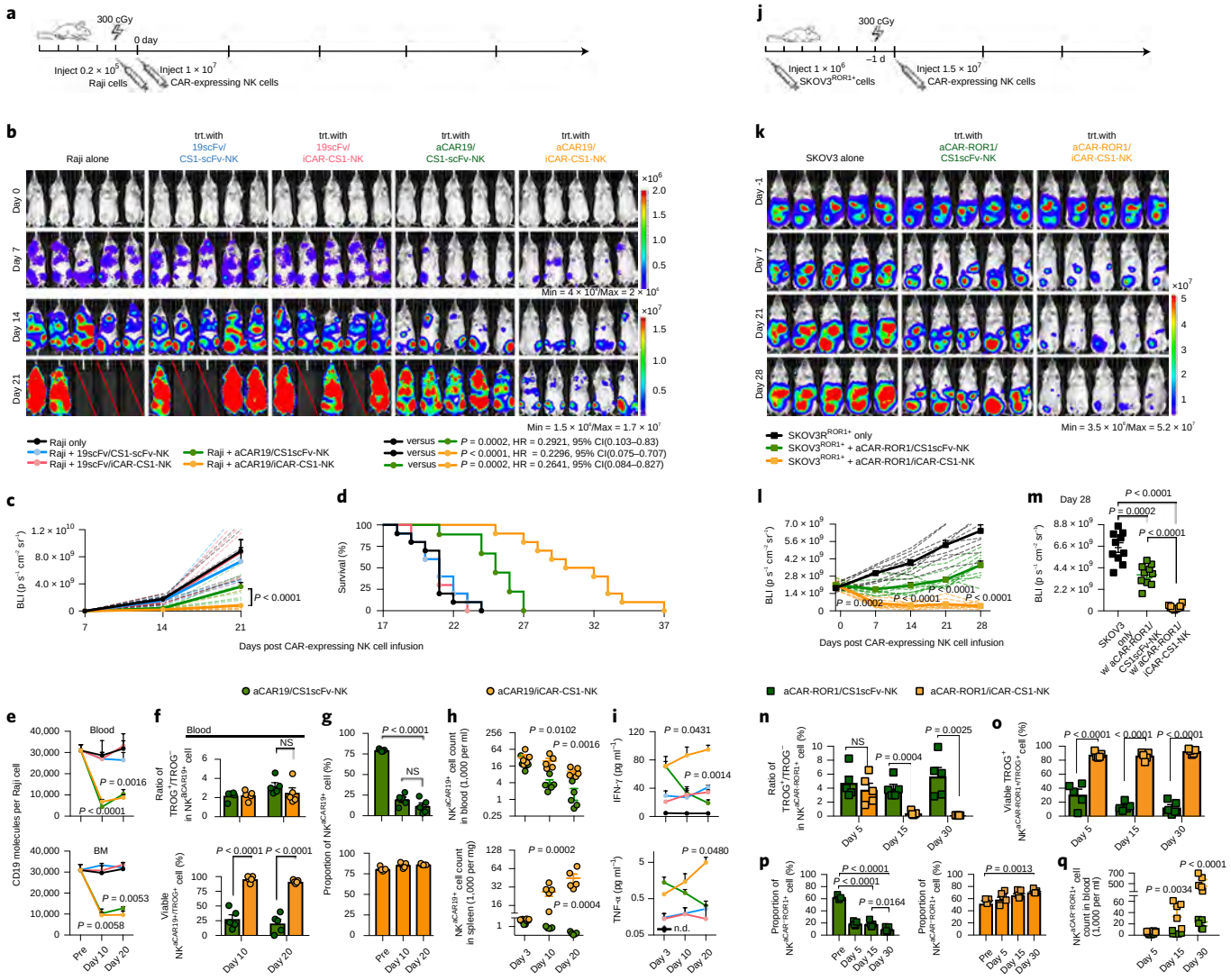

Fig. 6 | AI-CAR-expressing NK cells showed superior in vivo antitumor activity. a, Schema of the mouse model of Raji tumor. Mice received a single infusion of NK cells expressing 19scFv/CS1scFv (blue), 19scFv/iCAR-CS1 (red), aCAR19/CS1scFv (green) or aCAR19/iCAR-CS1 (orange). trt, treatment; $n=5$ mice. **b**,**c**, Tumor burden was assessed weekly by BLI (**b**), and presented as the normalized intensity of BLI (**c**); dashed lines refer to each mouse. **d**, Kaplan–Meier curves showing survival of mice. **e**, CD19 expression on Raji cells (molecule count per cell) in peripheral blood (PB) and bone marrow (BM), controlled against tumor only ($n=5$ mice). **f**, tCD19 expression on singlet NK^{CAR19+} cells, indicated as $TROG^+/TROG^-$ ratio (upper), and viability (%) of $TROG^+$ fraction (NK^{tCD19+}, lower) for aCAR19/CS1scFv versus aCAR19/iCAR-CS1 NK cells, in PB ($n=5$ mice per group). **g**, NK cell viability in PB after aCAR19/iCAR1-CS1 (green bars, upper) or aCAR19/CS1scFv NK cell infusion (orange bars, lower; $n=5$ mice per group). **h**, Viable $NK^{aCAR19+}$ cell count in PB and spleen ($n=5$ mice per group). **i**, Serum IFN-γ and TNF-α levels ($n=5$ mice per group). **j**, Schema of $SKOV3^{ROR1+}$ engrafted mouse model receiving a single infusion of NK cells expressing aCAR-ROR1/CS1scFv (green), or aCAR-ROR1/iCAR-CS1 (orange), with the nontreated tumor-engrafted group as control ($n=5$ mice per group). **k**–**m**, Weekly tumor burden assessment by BLI (**k**); the normalized BLI intensity for each mouse is indicated by dashed lines (**l**); and BLI intensity at day 28 (**m**). **n**, tROR1 expression on singlet $NK^{aCAR-ROR1+}$ cells (ratio of $TROG^+/TROG^-$). **o**, Percentage of viable $TROG^+$ fraction (NK^{tROR1+}) for aCAR-ROR1/CS1scFv (green bar) or aCAR-ROR1/iCAR-CS1 NK cells (orange bar) in PB ($n=5$ mice per group). **p**, Percentage of viable $GFP^-CD3^-CD56^+$aCAR-ROR1$^+$ NK cells in PB after aCAR-ROR1/CS1scFv (green bar, left) or aCAR-ROR1/iCAR-CS1 NK cell infusion (orange bar, right; $n=5$ mice per group). **q**, Viable $NK^{aCAR-ROR1+}$ cell count in PB after aCAR-ROR1/CS1scFv (green symbols) or aCAR-ROR1/iCAR-CS1 cell infusion (orange symbols; $n=5$ mice per group). *P* values were determined by two-tailed two-way ANOVA in **c**, log-rank test in **d** or two-tailed Student's *t*-test in **e**–**i** and **l**–**q**. Data were pooled from two independent experiments using NK cells from different donors in **c**, **d**, **i** and **m**. Flow cytometry data are shown as mean + s.e.m. Each symbol represents an individual mouse sample. 95% CI, 95% confidence interval; w/, with.

against the tumor target. NK cells transduced with this AI-CAR system were less susceptible to TROG-antigen-mediated fratricide, and mediated a superior antitumor response both in vitro and in multiple in vivo models.

Together, this study reports aCAR-mediated trogocytosis, which contributes to a reduction in target antigen density, and NK cell fratricide and hyporesponsiveness, as a mechanism of disease relapse after aCAR-NK cell therapy. We provide a proof-of-concept approach to preventing aCAR-NK cells from TROG-antigen-induced immunomodulatory consequences using antigen-specific inhibitory KIR-based receptors (iCARs) that successfully inhibit aCAR-mediated TROG-antigen-induced NK cell fratricide, while retaining critical effector function against tumor cells expressing the same antigen. This dynamic modulation of

AI-CAR signaling may find useful applications to improve the in vivo persistence and therapeutic efficacy of a range of adoptive NK cell therapies.

Online content

Any methods, additional references, Nature Research reporting summaries, source data, extended data, supplementary information, acknowledgements, peer review information; details of author contributions and competing interests; and statements of data and code availability are available at https://doi.org/10.1038/s41591-022-02003-x.

Received: 15 December 2021; Accepted: 9 August 2022;
Published online: 29 September 2022

References

1. Joly, E. & Hudrisier, D. What is trogocytosis and what is its purpose? *Nat. Immunol.* **4**, 815 (2003).
2. Dance, A. Core concept: cells nibble one another via the under-appreciated process of trogocytosis. *Proc. Natl Acad. Sci. USA* **116**, 17608–17610 (2019).
3. Bettadapur, A., Miller, H. W. & Ralston, K. S. Biting off what can be chewed: trogocytosis in health, infection, and disease. *Infect. Immun.* **88**, e00930-19 (2020).
4. Ahmed, K. A., Munegowda, M. A., Xie, Y. & Xiang, J. Intercellular trogocytosis plays an important role in modulation of immune responses. *Cell Mol. Immunol.* **5**, 261–269 (2008).
5. Miyake, K. & Karasuyama, H. The role of trogocytosis in the modulation of immune cell functions. *Cells* **10**, 1255 (2021).
6. Alhajjat, A. M. et al. Trogocytosis as a mechanistic link between chimerism and prenatal tolerance. *Chimerism* **4**, 126–131 (2013).
7. Ford McIntyre, M. S., Young, K. J., Gao, J., Joe, B. & Zhang, L. Cutting edge: in vivo trogocytosis as a mechanism of double negative regulatory T cell-mediated antigen-specific suppression. *J. Immunol.* **181**, 2271–2275 (2008).
8. Hamieh, M. et al. CAR T cell trogocytosis and cooperative killing regulate tumour antigen escape. *Nature* **568**, 112–116 (2019).
9. Cheng, M., Chen, Y., Xiao, W., Sun, R. & Tian, Z. NK cell-based immunotherapy for malignant diseases. *Cell Mol. Immunol.* **10**, 230–252 (2013).
10. Fang, F., Xiao, W. & Tian, Z. NK cell-based immunotherapy for cancer. *Semin. Immunol.* **31**, 37–54 (2017).
11. Myers, J. A. & Miller, J. S. Exploring the NK cell platform for cancer immunotherapy. *Nat. Rev. Clin. Oncol.* **18**, 85–100 (2021).
12. Koehl, U. et al. Advances in clinical NK cell studies: donor selection, manufacturing and quality control. *Oncoimmunology* **5**, e1115178 (2016).
13. Daher, M., Melo Garcia, L., Li, Y. & Rezvani, K. CAR-NK cells: the next wave of cellular therapy for cancer. *Clin. Transl. Immunol.* **10**, e1274 (2021).
14. Li, Y., Hermanson, D. L., Moriarity, B. S. & Kaufman, D. S. Human iPSC-derived natural killer cells engineered with chimeric antigen receptors enhance anti-tumor activity. *Cell Stem Cell* **23**, 181–192.e5 (2018).
15. Caumartin, J. et al. Trogocytosis-based generation of suppressive NK cells. *EMBO J.* **26**, 1423–1433 (2007).
16. Nakamura, K. et al. Fratricide of natural killer cells dressed with tumor-derived NKG2D ligand. *Proc. Natl Acad. Sci. USA* **110**, 9421–9426 (2013).
17. Domaica, C. I. et al. Tumour-experienced T cells promote NK cell activity through trogocytosis of NKG2D and NKp46 ligands. *EMBO Rep.* **10**, 908–915 (2009).
18. Lu, T. et al. Hijacking TYRO3 from tumor cells via trogocytosis enhances NK-cell effector functions and proliferation. *Cancer Immunol. Res.* **10**, 1229–1241 (2021).
19. Miner, C. A., Giri, T. K., Meyer, C. E., Shabsovich, M. & Tripathy, S. K. Acquisition of activation receptor ligand by trogocytosis renders NK cells hyporesponsive. *J. Immunol.* **194**, 1945–1953 (2015).
20. Elliott, J. M. & Yokoyama, W. M. Unifying concepts of MHC-dependent natural killer cell education. *Trends Immunol.* **32**, 364–372 (2011).
21. Anfossi, N. et al. Human NK cell education by inhibitory receptors for MHC class I. *Immunity* **25**, 331–342 (2006).
22. Bryceson, Y. T. & Long, E. O. Line of attack: NK cell specificity and integration of signals. *Curr. Opin. Immunol.* **20**, 344–352 (2008).
23. Pegram, H. J., Andrews, D. M., Smyth, M. J., Darcy, P. K. & Kershaw, M. H. Activating and inhibitory receptors of natural killer cells. *Immunol. Cell Biol.* **89**, 216–224 (2011).
24. Hudrisier, D., Aucher, A., Puaux, A. L., Bordier, C. & Joly, E. Capture of target cell membrane components via trogocytosis is triggered by a selected set of surface molecules on T or B cells. *J. Immunol.* **178**, 3637–3647 (2007).
25. Alter, G., Malenfant, J. M. & Altfeld, M. CD107a as a functional marker for the identification of natural killer cell activity. *J. Immunol. Methods* **294**, 15–22 (2004).
26. Poorebrahim, M. et al. Counteracting CAR T cell dysfunction. *Oncogene* **40**, 421–435 (2021).
27. Judge, S. J., Murphy, W. J. & Canter, R. J. Characterizing the dysfunctional NK cell: assessing the clinical relevance of exhaustion, anergy, and senescence. *Front. Cell. Infect. Microbiol.* **10**, 49 (2020).
28. Good, C. R. et al. An NK-like CAR T cell transition in CAR T cell dysfunction. *Cell* **184**, 6081–6100.e26 (2021).
29. Pesce, S. et al. Identification of a subset of human natural killer cells expressing high levels of programmed death 1: a phenotypic and functional characterization. *J. Allergy Clin. Immunol.* **139**, 335–346 e333 (2017).
30. Anderson, A. C., Joller, N. & Kuchroo, V. K. Lag-3, Tim-3, and TIGIT: co-inhibitory receptors with specialized functions in immune regulation. *Immunity* **44**, 989–1004 (2016).
31. Gill, S. et al. Rapid development of exhaustion and down-regulation of eomesodermin limit the antitumor activity of adoptively transferred murine natural killer cells. *Blood* **119**, 5758–5768 (2012).
32. Myers, J. A. et al. Balanced engagement of activating and inhibitory receptors mitigates human NK cell exhaustion. *JCI Insight* **7**, e150079 (2022).
33. Simonetta, F., Pradier, A. & Roosnek, E. T-bet and eomesodermin in NK cell development, maturation, and function. *Front. Immunol.* **7**, 241 (2016).
34. Gardiner, C. M. & Finlay, D. K. What fuels natural killers? Metabolism and NK cell responses. *Front. Immunol.* **8**, 367 (2017).
35. O'Brien, K. L. & Finlay, D. K. Immunometabolism and natural killer cell responses. *Nat. Rev. Immunol.* **19**, 282–290 (2019).
36. Liu, E. et al. Cord blood NK cells engineered to express IL-15 and a CD19-targeted CAR show long-term persistence and potent antitumor activity. *Leukemia* **32**, 520–531 (2018).
37. Daher, M. et al. Targeting a cytokine checkpoint enhances the fitness of armored cord blood CAR-NK cells. *Blood* **137**, 624–636 (2021).
38. Li, L. et al. A novel immature natural killer cell subpopulation predicts relapse after cord blood transplantation. *Blood Adv.* **3**, 4117–4130 (2019).
39. Merino, A. et al. Chronic stimulation drives human NK cell dysfunction and epigenetic reprograming. *J. Clin. Invest.* **129**, 3770–3785 (2019).
40. Van Gassen, S. et al. FlowSOM: using self-organizing maps for visualization and interpretation of cytometry data. *Cytometry A* **87**, 636–645 (2015).
41. Liu, E. et al. Use of CAR-transduced natural killer cells in CD19-positive lymphoid tumors. *N. Engl. J. Med.* **382**, 545–553 (2020).
42. Vivier, E., Nunes, J. A. & Vely, F. Natural killer cell signaling pathways. *Science* **306**, 1517–1519 (2004).
43. Kirwan, S. E. & Burshtyn, D. N. Killer cell Ig-like receptor-dependent signaling by Ig-like transcript 2 (ILT2/CD85j/LILRB1/LIR-1). *J. Immunol.* **175**, 5006–5015 (2005).
44. Zenarruzabeitia, O., Vitalle, J., Eguizabal, C., Simhadri, V. R. & Borrego, F. The biology and disease relevance of CD300a, an inhibitory receptor for phosphatidylserine and phosphatidylethanolamine. *J. Immunol.* **194**, 5053–5060 (2015).
45. Andre, P. et al. Anti-NKG2A mAb is a checkpoint inhibitor that promotes anti-tumor immunity by unleashing both T and NK cells. *Cell* **175**, 1731–1743.e13 (2018).
46. Meyaard, L. et al. LAIR-1, a novel inhibitory receptor expressed on human mononuclear leukocytes. *Immunity* **7**, 283–290 (1997).
47. Wu, Z. et al. Dynamic variability in SHP-1 abundance determines natural killer cell responsiveness. *Sci. Signal.* **14**, eabe5380 (2021).
48. Long, E. O., Kim, H. S., Liu, D., Peterson, M. E. & Rajagopalan, S. Controlling natural killer cell responses: integration of signals for activation and inhibition. *Annu. Rev. Immunol.* **31**, 227–258 (2013).
49. Tai, Y. T. et al. Anti-CS1 humanized monoclonal antibody HuLuc63 inhibits myeloma cell adhesion and induces antibody-dependent cellular cytotoxicity in the bone marrow milieu. *Blood* **112**, 1329–1337 (2008).
50. Hsi, E. D. et al. CS1, a potential new therapeutic antibody target for the treatment of multiple myeloma. *Clin. Cancer Res.* **14**, 2775–2784 (2008).
51. Ma, X. et al. Pan-cancer genome and transcriptome analyses of 1,699 paediatric leukaemias and solid tumours. *Nature* **555**, 371–376 (2018).
52. Lohr, J. G. et al. Discovery and prioritization of somatic mutations in diffuse large B-cell lymphoma (DLBCL) by whole-exome sequencing. *Proc. Natl Acad. Sci. USA* **109**, 3879–3884 (2012).
53. Olson, M. L. et al. Low-affinity CAR T cells exhibit reduced trogocytosis, preventing rapid antigen loss, and increasing CAR T cell expansion. *Leukemia* **36**, 943–1946 (2022).
54. Hochreiter-Hufford, A. & Ravichandran, K. S. Clearing the dead: apoptotic cell sensing, recognition, engulfment, and digestion. *Cold Spring Harb. Perspect. Biol.* **5**, a008748 (2013).
55. Kalluri, R. & LeBleu, V. S. The biology, function, and biomedical applications of exosomes. *Science* **367**, eaau6977 (2020).
56. Tabiasco, J. et al. Acquisition of viral receptor by NK cells through immunological synapse. *J. Immunol.* **170**, 5993–5998 (2003).
57. Tabiasco, J. et al. Active trans-synaptic capture of membrane fragments by natural killer cells. *Eur. J. Immunol.* **32**, 1502–1508 (2002).

58. Nakamura, K. et al. NK-cell fratricide: dynamic crosstalk between NK and cancer cells. *Oncoimmunology* **2**, e26529 (2013).
59. Carlsten, M. et al. Checkpoint inhibition of KIR2D with the monoclonal antibody IPH2101 induces contraction and hyporesponsiveness of NK cells in patients with myeloma. *Clin. Cancer Res.* **22**, 5211–5222 (2016).
60. Taylor, R. P. & Lindorfer, M. A. Fcγ-receptor-mediated trogocytosis impacts mAb-based therapies: historical precedence and recent developments. *Blood* **125**, 762–766 (2015).

Methods

Cell lines, primary cells and culture conditions. CD19$^+$ cell lines of Raji (CCL-86), NALM-6 (CRL-3273) and Ramos (CRL-1596); CD5$^+$ cell line CCRF (CRM-CCL-119); CD70$^+$ cell line THP-1 (TIB-202); CD123$^+$ cell line MOLM-14 (ACC 777); BCMA$^+$ cell line MM1S (CRL-2974); SKOV3 cell line (HTB-77); K562 cell line (CRL-3344); and 293T cell line (CRL-3216) were obtained from the American Type Culture Collection. Raji, NALM-6, Ramos, CCRF, MOLM-14 and K562 cells were cultured in RPMI-1640 (Invitrogen) supplemented with 10% FBS (HyClone), 1% penicillin-streptomycin and 1% GlutaMAX; THP-1 and 293T cells were cultured in DMEM (Invitrogen) supplemented with 10% FBS, 1% penicillin-streptomycin and 1% GlutaMAX; SKOV3 cells were cultured in McCoy's 5a Medium (Invitrogen) supplemented with 10% FBS, 1% penicillin-streptomycin and 1% GlutaMAX. K562 cells were retrovirally transduced to co-express 4-1BBL, CD48 and membrane-bound IL-21 and served as uAPCs for in vitro NK cell expansion[61]. To model trogocytosis detection by using a fluorescent-traceable marker, the *CD19* gene in Raji cells was deleted using the CRISPR–Cas9 system (crRNA1: CTAGGTCCGAAACATTCCAC-CGG; crRNA2: CGAGGAACCTCTAGTGGTGA-AGG); CD19-knockout Raji (Raji$^{CD19\text{-}KO}$) cells were purified by MoFlo Astrios (Beckmen Coulter) and then retrovirally transduced to express CD19–mCherry fusion protein with or without GFP co-expression (Raji$^{CD19\text{–}mCherry/GFP}$ and Raji$^{CD19\text{–}mCherry}$). Raji cells were transduced with firefly luciferase-GFP to allow in vivo tumor burden examination using the IVIS Spectrum imaging system (Caliper). To have an in vivo model of solid tumors with target antigen CD19 expression, SKOV3 cells were genetically modified (SKOV3^{gCD19+}) and labeled with firefly luciferase-GFP. All cells were maintained in a 37 °C incubator with 5% CO_2, and regularly tested for mycoplasma contamination using the MycoAlert Mycoplasma Detection Kit (Lonza).

Peripheral blood mononuclear cells from patients treated with CAR19/IL-15 NK cells. Clinical samples used in this study were collected from patients treated in a clinical trial of iC9/CAR19/IL-15 (CAR19/IL-15)-transduced cord blood NK (CB-NK) cells, as previously reported (NCT03056339)[41]. Peripheral blood mononuclear cells from 11 patients with CLL or non-Hodgkin lymphoma were collected at different time points following CAR19/IL-15 NK cell adoptive therapy at MD Anderson Cancer Center (MDACC). The normalized mean TROG-CD19 (tCD19) geometric mean fluorescence intensity (gMFI) on CAR19-NK cells for the whole patient cohort was 6.29 (range of 0.61–35.77). Patients with a high (>mean) versus low (≤mean) normalized tCD19 gMFI at more than one time point were defined as group TROG^{high} ($n=4$ patients) versus TROG^{low} ($n=7$ patients), respectively. In addition, circulating leukemia cells from four patients with CLL and four patients with B cell ALL enrolled on laboratory protocols were isolated after density-gradient centrifugation for in vitro studies of trogocytosis. All patients gave informed consent per the Institutional Review Board (IRB). All studies were performed in accordance with the Declaration of Helsinki.

Vector constructs and retrovirus production. The retroviral vector encoding iCas9, 19scFv.CD28.zeta.2A.IL-15 (CAR19/IL-15), was kindly provided by Dr Gianpietro Dotti (University of North Carolina, Chapel Hill)[62]. The iCas9.19scFv.2A.IL-15 (19scFv/IL-15), iCas9.CD5scFv (XZ-CD5 (ref. [63])). CD28.zeta.2A.IL-15 (CAR5/IL-15), iCas9.CD5scFv.DAP10.zeta.2A.IL-15 (CAR(DAP10z)/IL-15), iCas9.CD5scFv.zeta.2A.IL-15 (CAR(3z)/IL-15), iCas9.CD5scFv.DAP12.zeta.2A.IL-15 (CAR(DAP12z)/IL-15), iCas9.CD5scFv.NKG2D.zeta.2A.IL-15 (CAR(2Dz)/IL-15), iCas9.CD5scFv.41BB.zeta.2A.IL-15 (CAR(BBz)/IL-15), iCas9.CD5scFv.DAP10.2A.IL-15 (CAR(DAP10)/IL-15), iCas9.CD5scFv.DAP12.2A.IL-15 (CAR(dap12)/IL-15), iCas9.CD70scFv (ARGX-110 (ref. [64]) or LB no. 14).CD28.zeta.2A.IL-15 (CAR70/IL-15), iCas9.CD27(ECD).CD28.zeta.2A.IL-15 (CAR27s/IL-15), iCas9.CD123scFv (26292 (ref. [65])).CD28.zeta.2A.IL-15 (CAR123/IL-15) and iCas9.BCMAscFv (huc11D5.3-Luc90 (ref. [66])). CD28.zeta.2A.IL-15 (CAR-BCMA/IL-15) constructs were cloned into the SFG retroviral backbone to generate additional viral vectors. For the construction of iCARs, transmembrane domains of KIR2DL1 and LIR-1, and cytoplasmic signaling domains of KIR2DL1, LIR-1, LAIR-1, NKG2A and CD300A were used as inhibitory signals. Extracellular domains comprising either 19scFv or CS1scFv (HuLuc63 (ref. [49])), along with IgG hinge, were used to fuse and generate iCAR19 or iCAR-CS1 constructs, respectively. CS1scFv, iCAR-CS1 and iCAR19/IL-15 constructs were then each cloned into the SFG retroviral backbone. The whole CD19 coding sequence was fused to an mCherry reporter gene at the 3′ end to generate the CD19–mCherry construct. CD19–mCherry and GFP were then linked using the 2A peptide, resulting in the bicistronic CD19–mCherry/GFP construct. mCherry, CD19–mCherry and CD19–mCherry/GFP were also each cloned into the SFG retroviral backbone. All construct syntheses and molecular cloning were performed by GeneArt Gene Synthesis (Thermo Fisher Scientific). Transient retroviral supernatants were produced from transfected 293T cells as previously described[67].

CB-NK cell transduction and expansion. Cord blood units for research were provided by the MDACC CB Bank under an IRB-approved protocol (Lab04-0249). CB-NK cells were isolated and expanded as previously described[36]. In brief, lymphocytes were collected by density-gradient centrifugation using Ficoll-Histopaque solution (Sigma-Aldrich). CD56$^+$CD3$^-$ NK cells were then purified using an NK negative isolation kit (Miltenyi Biotec), and cocultured with irradiated (100 Gy) uAPCs at a 2:1 ratio in complete stem cell growth medium, supplemented with 200 U ml^{-1} recombinant human IL-2 (Proleukin). On day 4 post uAPC stimulation, fresh NK cells were purified again and transduced with retroviral vectors expressing CAR constructs. A second retroviral transduction of iCAR constructs was performed on day 6 to then generate NK cells expressing AI-CAR. Following the same approach, CD19–mCherry- or CD19–mCherry/GFP-expressing cells (both primary NK cells and tumor cells) were prepared. CAR transduction efficiency was measured by flow cytometry. Irradiated uAPCs were added weekly to the NK cell culture to support NK cell expansion.

Flow cytometry. CAR expression was measured by detection of IgG hinge using conjugated goat anti-human lgG (H+L; Jackson ImmunoResearch). For AI-CAR detection, anti-CD19 aCAR expression was measured using the CD19 CAR detection reagent (Miltenyi Biotec). Expression of anti-CS1 iCAR was measured by binding of CAR to CS1 His-tag fusion protein (ACRO Biosystems). Ghost Dye Violet 450 (TONBO Biosciences) was used to determine viability, and Aqua fixable viability dye (eBioscience) was used for assessing viability when fixation protocols were applied. Human Fc receptor-blocking solution (Miltenyi Biotec) was used to block Fc receptors to minimize nontargeted specific staining. For intracellular staining, cells were fixed and permeabilized using Intracellular Fixation and Permeabilization Buffer Kit (eBioscience) according to the manufacturer's protocol. For phosphoflow staining, cells were prepared and fixed using the Perfix Expose Kit from Beckman Coulter, according to the manufacturer's protocol. Phycoerythrin Fluorescence Quantitation Kit (BD Biosciences) was used according to the manufacturer's protocol to determine the number of molecules of CD19, CD5, CD70, CD123 and BCMA per cell. AccuCheck Counting Beads (ThermoFisher) were used to determine the cell concentration in each tested population. Amnis Imagestream-X MarkII (Millipore) was used to visualize fixed cells at ×60 magnification with a pixel size of 0.1 μm^2; data were analyzed using IDEAS (Millipore). Flow cytometry analysis was performed on an LSRFortessa X-20 (BD Bioscience) and data were analyzed using FlowJo (BD Bioscience). Cell sorting was performed using a MoFlo XDP cell sorter (Beckman Coulter). Antibodies used for flow cytometry analysis include: CD45-Krome Orange (1:40), CD56-BV650 (1:200), CD16-BV605 (1:100), Anti-His Tag-PE (1:100), CD19-APC (1:100), CD20-APC (1:100), CD19-BV785 (1:100), CD3-APC-H7 (1:200), CD19-PE (1:100), Biotin-APC (1:100), CD20-PerCP/Cyanine5.5 (1:100), CD22-PerCP/Cyanine5.5 (1:100), CD22-APC (1:100), GFP-AF488 (1:100), Fixable Viability Dye-eFluor 506 (1:200), CD319-PE/Cyanine7 (1:100), CD366-PE/Cyanine7 (1:100), CD223-BV785 (1:100), TIGIT-BV421 (1:100), CD279-PE (1:100), Isotype-PE (1:100), Isotype-BV786 (1:100), EOMES-PerCP (1:100), T-bet-PE (1:100), LIVE/DEAD Fixable Aqua Dead Cell Stain (1:200), ROR1-PE (1:100), Human BD Fc Block (1:200), CD19-PerCP (1:100), Perforin-AF647 (1:100), CD107a-BV785 (1:100), TNF-α-PE/Cyanine7 (1:100), IFN-γ-V450 (1:100), Zap70 (Y319)/Syk (Y352)-PE (1:100), ROR1 Protein/His Tag (1:100), SLAMF Protein/His Tag (1:100), Biotinylated Human CD19 (20-291) Protein (1:100), pSHP-1-PE (1:100), Phalloidin-AF647 (1:10,000), CD56-PE/Cyanine7 (1:50), CD19-AF594 (1:50), CD20-APC/Cyanine7 (1:50), CD22-APC/Cyanine7 (1:50) and Gt F(ab')$_2$- PE (1:200).

Trogocytosis assay. NK cells were cocultured with designated GFP$^+$ target cells at an E:T ratio of 1:1. Cocultured cells were washed with FACS buffer and then subjected to surface staining of anti-hCD56 (Biolegend, HCD56, 1:200) and anti-hCD3 (Biolegend, SK7, 1:200) antibodies at 4 °C for 20 min in the dark. Following staining, cells were washed and assessed by flow cytometry. The TROG$^+$ population was defined by the detection of TROG-antigen on the surface of singlet NK (CD56$^+$CD3$^-$GFP$^-$) cells; also, the cognate antigen expression on the cocultured tumor cells (CD56$^-$GFP$^+$) was evaluated. The Incucyte Live-Cell Analysis System (ESSEN Bioscience) was used for the mCherry-based trogocytosis assay, where Raji$^{CD19\text{–}mCherry}$ cells or Raji^{mCherry} cells were cocultured with carboxy fluorescein succinimidyl ester (CFSE) (ThermoFisher)-labeled NK cells at a 1:1 ratio. Image scanning of the mCherry signal in NK cells was recorded in real-time and cells that showed both mCherry and CFSE signals were identified as the NK^{TROG+} population. To block trogocytosis, NK cells were pre-treated with 1 μM LatA (Sigma-Aldrich) at 37 °C for 20 min before coculture with target cells.

NK activation assay. NK cells were stimulated by target cells at an E:T ratio of 1:1 for 6 h. To inhibit protein transport, GolgiStop and GolgiPlug (BD Bioscience) were added to the culture at the second hour post-coculture according to the manufacturer's protocol. Anti-CD107a (Biolegend, H4A3, 1:100) was also added at this time point to capture CD107a as a marker of NK cell degranulation. When examining NK^{TROG+} cell populations, GolgiStop and GolgiPlug were not added to allow the trogocytosis. After incubation, cells were washed with FACS buffer (BD Bioscience) and stained with anti-hCD56, anti-hCD3. Ghost Dye Violet 450 (Tonbo Biology, 1:200) was used to identify the viability of NK populations. Intracellular staining was with IFN-γ (BD Bioscience, B27, 1:100) and tumor necrosis factor-α (TNF-α) (BD Bioscience; MAb11 antibodies were subsequently applied, 1:100). Expression of CD107a, IFN-γ and TNF-α was measured

and expressed as a percentage of $CD56^+CD3^-$ NK cells when compared with unstimulated NK cells.

Cytotoxicity assay in Incucyte system. NK cells were cocultured at an E:T ratio of 1:1 with tumor cells either labeled with Vybrant DyeCycle Ruby Stain (ThermoFisher) or expressing mCherry signal. The Incucyte caspase-3/7 green apoptosis assay reagent (SAETORIUS) was added to each well to label apoptotic cells. Images of each well were captured in real-time during the period of 6–30-h post-addition. Data were analyzed using the Incucyte Live-Cell Analysis System which assessed the number of apoptotic cells (green) and target cells (red) in a real-time manner. The percentage of caspase-3/7 expression was measured in cells showing both green and red signals, and computed as an expression of the total detected target cells (red). CD19 scFv antibody (200 ng ml^{-1}, Invivogen) was pre-incubated with NK^{TROG+} populations for 30 min to block CD19 antigen exposure, and anti-β-Gal scFv antibody (200 ng ml^{-1}, Invivogen) was used as the negative control.

Single-cell cytotoxicity assay. Time-lapse imaging microscopy in Nanowell grids (TIMING) was used to test NK-mediated cytotoxicity at a single-cell scale as previously described[68]. In brief, the sorted NK cell populations and target cells (K562 or Raji) were labeled with lipophilic PKH dyes, respectively, and loaded onto Nanowell arrays. The array was incubated with medium that was pre-mixed with Annexin V (BD Bioscience), and monitored in real-time for 5–6 h by a Carl Zeiss Axio Observer fitted with a Hamamatsu Orca-Flash sCMOS camera using a ×20, 0.8 numerical aperture objective. Images of ~5,000 wells were collected and processed using an in-house algorithm for cell tracking and segmentation[69].

NK population doubling assay. CB-NK cells were subcultured every week, with or without uAPC feeder cells, after the initial transduction and expansion. Using the equation population doubling = $\log_{10}[(A/B)/2]$, where A is the number of collected cells and B the number of plated cells from each subculture, the weekly population doubling was measured. Then, the sum of each population doubling over time was determined as the cumulative population doublings. Assays were terminated 3 weeks after the cell count from the subculture failed to achieve at least an equal amount of seeded cells. Data were obtained from three different CB-NK populations for each condition.

Mass cytometry (CyTOF). Mass cytometry was performed as previously described[37,38]. Primary antibodies were conjugated in-house with corresponding metal tags using MaxparX8 polymer antibody labeling kit per the manufacturer's protocol (Fludigm). NK cells were washed with cell staining buffer (0.5% BSA/PBS), and incubated with human Fc receptor-blocking solution (Miltenyi Biotec) before antibody mix was added. Cells were then incubated with 2.5 μM cisplatin (Sigma-Aldrich), followed by fixation and permeabilization using BD Cytofix/Cytoperm solution according to the manufacturer's protocol. For intracellular staining, cells were washed twice with perm/wash buffer and incubated directly with antibody master mix against intracellular markers. Cells were then stored overnight in 500 μl of 1.6% paraformaldehyde (EMD Milipore)/PBS with 125 nM iridium nucleic acid intercalator (Fluidigm). On the days that cells were assessed, they were washed in 1 ml of MilliQ dH_2O, and filtered through a 35 μm nylon mesh (cell strainer cap tubes, BD Bioscience). The cells were then resuspended in MilliQ dH_2O supplemented with EQ Four Element Calibration Beads, and subsequently acquired at 300 events per second on a Helios instrument (Fluidigm).

For CyTOF analysis, antibodies used with the corresponding metal tag isotopes for in vitro experiments include: CD45 (Fluidigm, HI30, ^{89}Y), GFP (Biolegend, FM264G, ^{144}Nd), DAP12 (RD, 406288, ^{146}Nd), NKG2C (Biolegend, 134591, ^{147}Sm), TRAIL (Miltenyi, REA1113, ^{148}Nd), CD25 (Miltenyi, REA570, ^{149}Sm), CD69 (Biolegend, FN50, ^{150}Nd), CD2 (Miltenyi, REA972, ^{151}Eu), CAR (Jackson ImmunoResearch, polyclonal, ^{152}Sm), PAN-KIR (RD, 180704, ^{153}Eu), TIGIT (ThermoFisher, MBSA43, ^{154}Sm), KLRG1 (Miltenyi, REA261, ^{156}Gd), OX40 (Miltenyi, REA621, ^{158}Gd), Perforin (Miltenyi, REA1061, ^{159}Tb), PD1 (Miltenyi, PD1.3.1.3, ^{160}Gd), EOMES (ThermoFisher, WD1928, ^{161}Dy), T-bet (Miltenyi, 4B10, ^{162}Dy), c-Kit (Miltenyi, REA787, ^{163}Dy), SAP (Biolegend, 1A9, ^{164}Dy), TIM3 (RD, 344823, ^{165}Ho), NKG2D (Miltenyi, REA797, ^{166}Er), 2B4 (ThermoFisher, C1.7, ^{167}Er), Ki67 (Biolegend, Ki67, ^{168}Er), NKG2A (Miltenyi, REA110, ^{169}Tm), DNAM-1 (Miltenyi, REA1040, ^{170}Er), CS1 (Biolegend, 162.1, ^{172}Yb), Granzyme B (Miltenyi, REA226, ^{173}Yb), CD94 (Miltenyi, REA113, ^{174}Yb), LAG3 (Miltenyi, REA351, ^{175}Lu), ICOS (Miltenyi, REA192, ^{176}Yb), CD16 (Fluidigm, 3G8, ^{209}Bi), CD3 (Biolegend, UCHT1, ^{194}Pt), Cisplatin L/D (Fluidigm, ^{198}Pt), CD56 (BD Bioscience, NCAM16.2, ^{106}Cd), CD19 (Biolegend, HIB19, ^{110}Cd), Granzyme A (Miltenyi, REA162, ^{111}Cd), Syk (Biolegend, 4D10.2, ^{112}Cd), NKp30 (Miltenyi, AF29-4D12, ^{113}Cd), NKp46 (Miltenyi, REA808, ^{114}Cd), NKp44 (Miltenyi, REA1163, ^{116}Cd). Antibodies used with the corresponding metal tag isotopes for in vivo experiments include: CD45 (Biolegend, HI30, ^{89}Y), CD2 (Biolegend, TS1/8, ^{141}Pr), CD62L (BD Biosciences, DREG-56, ^{143}Nd), CD27 (Biolegend, M-T271, ^{144}Nd), CD56 (Biolegend, HCD56, ^{146}Nd), NKG2C (RD, 134591, ^{147}Sm), CXCR6 (RD, 56811, ^{148}Nd), CXCR3 (RD, 49801, ^{149}Sm), Granzyme B (RD, polyclonal, ^{150}Nd), T-bet (Biolegend, 4B10, ^{151}Eu), TIGIT (Biolegend, A15153G, ^{152}Sm), Granzyme A (Biolegend, CB9, ^{154}Sm), NKG2A (RD, 131411, ^{155}Gd), TIM3 (Biolegend, F38-2E2, ^{156}Gd), CD19 (Biolegend, HIB19, ^{157}Gd), 2B4 (Biolegend, 2-69, ^{158}Gd), CLA (Biolegend, KPL-1, ^{159}Tb), CD20 (Biolegend, RIK-2, ^{160}Gd), DNAM-1 (Miltenyi, DX11, ^{161}Dy), EOMES (ThermoFisher, WD1928, ^{162}Dy), NKp30 (Biolegend, P30-15, ^{163}Dy), c-Kit (BD, YB5.B8, ^{164}Dy), CD25 (BD, 2A3, ^{165}Ho), NKG2D (RD, 149810, ^{166}Er), Perforin (BD, δG9, ^{167}Er), ZAP70 (ThermoFisher, 1E7.2, ^{168}Er), CCR5 (Biolegend, J418F1, ^{169}Tm), CAR (Jackson ImmunoResearch, polyclonal, ^{170}Er), CX3CR1 (Biolegend, 2A9-1, ^{171}Yb), CXCR1 (Biolegend, 8f1, ^{172}Yb), PD1 (Biolegend, EH12.2H7, ^{173}Yb), Syk (Biolegend, 4D10.2, ^{174}Yb), NKp46 (RD, 195314, ^{175}Lu), KLRG1 (ThermoFisher, 13F12F2, ^{176}Yb), CD57 (Biolegend, HNK-1, ^{194}Pt), Cisplatin L/D (Fluidigm, ^{198}Pt), CD16 (Fluidigm, 3G8, ^{209}Bi).

Mass cytometry data analysis. Mass cytometry data were analyzed using Cytobank. NK cell populations were identified by using the strategy of gating singlets in Pt195 $(cisplatin)^{low}$ $hCD45^+CD56^+CD3^-$, and were applied to all files. CAR^+ and $CD19^+$ expression was determined based on either isotype control or NK cells cultured alone as controls. Data from 10,000 identified NK cells per each in vitro sample were randomly subsampled in FlowJo. Normalized data from each sample were pooled and analyzed to acquire their variability in signals. A *t*-SNE map was generated by the *t*-SNE analysis that performed a pairwise comparison of cellular phenotypes to optimally plot clusters and reduce dimensions from multiple parameters. Subsequently, FlowSOM analysis was performed to determine metaclusters in optimized grouping distance between the empirically expected nodes and to build a minimum spanning tree by connecting nodes hierarchically. The expression of each marker was transformed and normalized locally, then hierarchically clustered, and plotted as a heatmap using Morpheus matrix visualization and analysis software (Broad Institute).

Metabolism assays. ECAR and OCR were measured in GFP-negative CAR-NK effector cells using Seahorse XF Cell Mito Stress Test Kit (Agilent), and Seahorse XF Glycolysis Stress Test Kit (Agilent) in an Agilent Seahorse XFe96 Analyzer according to the manufacturer's protocol. The assay was performed in phenol red/carbonate-free RPMI medium (Agilent) containing 2 nM l -glutamine (Agilent), 25 mM glucose and 2 mM pyruvate (Agilent, but excluded in the glycolysis assay). Cell mito stress test was performed by examining OCRs after administering 1.5 μM oligomycin, 0.5 μM fluorocarbonyl cyanide phenylhydrazone, 0.5 μM rotenone and antimycin A. The glycolysis test was measured as the ECAR following injection with 10 mM glucose, 1 μM oligomycin and 50 mM 2-deoxy-d-glucose.

CAR-NK cell affinity experiment. Experiments were performed using poly-l -lysine (Sigma-Aldrich)-coated z-Movi chips. $MM1S^{CD70+}$ cells were seeded onto a z-Movi chip, creating a monolayer. The z-Movi chip was then sealed and incubated in a dry incubator for 30 min. Effector cells were stained with Cell Trace Far Red (ThermoFisher) and their flow measured onto the monolayer, 200–500 cells at a time. Effectors were then incubated with the target cell monolayer for 5 min before the start of the force ramp. The force ramp was set at 1,000 pN over 90 s for each run. Affinity measurements were conducted on a z-Movi Cell Avidity Analyzer using the Oceon software.

Luminex assays. The MILLIPLEX MAP magnetic bead (Millipore) kit was used to measure human granzyme A, granzyme B, perforin, TNF-α and IFN-γ in serum collected from mice at different time points after receiving NK cell infusion as per the manufacturer's protocol. Measurements were performed on the Luminex 200 System.

Xenogeneic tumor-grafted mouse models. NOD/SCID IL-2Rγnull (NSG) mice grafted with aggressive, NK-resistant tumor cells were used to examine the antitumor activity of different NK populations as previously described[36,37]. Tumor models included $CD19^+$ Raji lymphoma, $CD5^+$ CCRF T-ALL, $CD123^+$ MOML14 acute myeloid leukemia and SKOV3 ovarian cancer. All experiments were performed in accordance with American Veterinary Medical Association and National Institutes of Health recommendations under protocols approved by the MDACC Institutional Animal Care and Use Committee (protocol number 00000889-RN02). Mice were maintained under specific-pathogen-free conditions, with a 12-h night/day cycle of light, and at stable ambient temperature with 40–70% relative humidity. Seven-week-old female NSG mice (Jackson Laboratories) were irradiated (300 cGy) on day −1. On day 0, firefly luciferase-GFP-labeled Raji cells were injected intravenously at three escalating dose levels of Raji cells (0.2×10^5, 1×10^5 or 5×10^5), respectively; for the other blood tumor models, one dose of $CCRF^{CD5+/Luci+/GFP+}$ cells (0.5×10^5) or $MOML14^{CD123+/Luci+/GFP+}$ cells (0.5×10^5) was injected intravenously, respectively. The mice were then serially treated with the indicated NK cell populations. For ovarian cancer models, 7-week-old female NSG mice (Jackson Laboratories) were injected intraperitoneally with luciferase-GFP-labeled SKOV3 cells (1×10^6 $SKOV3^{ROR1+}$ or 0.5×10^6 $SKOV3^{gCD19+}$) 7 days (day −7) before the treatment; at day −1, the mice were irradiated (300 cGy), and then received AI-CAR-expressing NK cells ($1–1.5\times10^7$) via intraperitoneal injection on day 0. BLI (Xenogen-IVIS 200 Imaging system; Caliper) was performed regularly to examine the engraftment of Raji cells and SKOV3 cells. Signal quantitation in photons per second was measured using IVIS Living Image software (Caliper Life Sciences). Hematoxylin and eosin and immunohistochemistry staining were performed on formalin-fixed

paraffin-embedded tumor tissue sections. The tumor tissues were fixed in 10% formalin, embedded in paraffin and serially sectioned. Then, 4-µm sections were used for the histopathological studies, and images were analyzed by ImageJ.

Statistics. Statistical analyses were performed and plotted using Prism v.7 software (GraphPad). The Student's *t*-test was used to test for significance; one-way ANOVA was applied to determine the comparison among groups at a certain condition; two-way ANOVA was applied to determine the comparison among groups in a time course; *P* value for pairwise comparisons was conservatively adjusted for multiple comparisons using Bonferroni correction. Mean values + s.e.m. are shown. The nonlinear regression model with the least trimmed sum of squares was selected as the robust goodness-of-fit[70]. Overall survival analysis was calculated using Kaplan–Meier methods and compared with the treatment group using log-rank tests with 95% confidence intervals.

Reporting summary. Further information on research design is available in the Nature Research Reporting Summary linked to this article.

Data availability

The human gene database GeneCard (genecards.org) was used to design the CAR constructs such as KIR2DL1 (GC19P067381), LIR-1 (GC19P067376), LAIR-1 (GC19M054351), NKG2A (GC12M021112) and CD300A (GC17P074466). Transcriptome data used in the generation of Extended Data Fig. 7g are available through the Gene Expression Omnibus (https://www.ncbi.nlm.nih.gov/geo/) under accession GSE190976. Source data are provided with this paper.

Code availability

No custom code was developed.

References

61. Liu, E. et al. GMP-compliant universal antigen presenting cells (uAPC) promote the metabolic fitness and antitumor activity of armored cord blood CAR-NK cells. *Front. Immunol.* **12**, 626098 (2021).
62. Hoyos, V. et al. Engineering CD19-specific T lymphocytes with interleukin-15 and a suicide gene to enhance their anti-lymphoma/leukemia effects and safety. *Leukemia* **24**, 1160–1170 (2010).
63. Przepiorka, D. et al. Evaluation of anti-CD5 ricin A chain immunoconjugate for prevention of acute graft-vs.-host disease after HLA-identical marrow transplantation. *Ther. Immunol.* **1**, 77–82 (1994).
64. Silence, K. et al. ARGX-110, a highly potent antibody targeting CD70, eliminates tumors via both enhanced ADCC and immune checkpoint blockade. *MAbs* **6**, 523–532 (2014).
65. Du, X., Ho, M. & Pastan, I. New immunotoxins targeting CD123, a stem cell antigen on acute myeloid leukemia cells. *J. Immunother.* **30**, 607–613 (2007).
66. Zah, E. et al. Systematically optimized BCMA/CS1 bispecific CAR-T cells robustly control heterogeneous multiple myeloma. *Nat. Commun.* **11**, 2283 (2020).
67. Vera, J. et al. T lymphocytes redirected against the κ light chain of human immunoglobulin efficiently kill mature B lymphocyte-derived malignant cells. *Blood* **108**, 3890–3897 (2006).
68. Liadi, I. et al. Individual motile CD4$^+$ T cells can participate in efficient multikilling through conjugation to multiple tumor cells. *Cancer Immunol. Res.* **3**, 473–482 (2015).
69. Merouane, A. et al. Automated profiling of individual cell–cell interactions from high-throughput time-lapse imaging microscopy in nanowell grids (TIMING). *Bioinformatics* **31**, 3189–3197 (2015).
70. Andreas, A., Christophe, C. & Sarah, G. Sparse least trimmed squares regression for analyzing high-dimensional large data sets. *Ann. Appl. Stat.* **7**, 226–248 (2013).

Acknowledgements

This work was supported in part by the generous philanthropic contributions to The University of Texas MD Anderson Cancer Center Moon Shots Program, and The Sally Cooper Murray endowment; and by grants (grant nos. 1 R01CA211044-01, 5 P01CA148600-03, P50CA100632-16 and R01GM143243) from the National Institutes of Health (NIH), CPRIT (grant no. RP180466), Stand Up To Cancer Dream Team Research (grant no. SU2C-AACR-DT-29–19) and the Leukemia Specialized Program of Research Excellence (SPORE) (grant no. P50CA100632); by a grant from the NIH to the MD Anderson Cancer Center Advanced Technology Genomics Core (ATGC) Facility (grant no. CA016672); and by the grant (no. P30 CA016672) from the NIH to the MD Anderson Cancer Center Flow Cytometry and Cellular Imaging Core Facility that assisted with the CyTOF studies. We thank E. Gokdemir, B. T. Whitfield and J. Lu for their technical assistance.

Author contributions

Y.L. and K.R. conceptualized the study, completed the experimental design, and interpreted and analyzed data. Y.L. directed in vitro experiments with assistance by G.W. Y.L., E.L., R.B., L.L. and L.N.K. executed animal works. Y.L., R.B., L.L. and N.U. performed mass cytometry experiments and analyses. Y.L., M.F., A.R. and N.V. executed single-cell imaging and analysis. P.P.B. collected clinical information. Y.L. drafted the original manuscript; B.L., A.B., H.R., X.G., L.M.G., P.L., S.A., D.M., M.D., M.S., M.M., S.A., L.B., R.E.C., E.E., N.V., K.C. and E.J.S. commented on the manuscript, which was reviewed and edited by J.S.M., T.J.L., L.M.-F., Y.L. and K.R.

Competing interests

R.B., E.L., L.N.K., P.P.B., S.A., D.M., M.D., R.E.C., E.J.S., K.R. and The University of Texas MD Anderson Cancer Center have an institutional financial conflict of interest with Takeda Pharmaceutical. S.A., D.M., R.B., E.L., L.N.K., E.J.S., K.R. and The University of Texas MD Anderson Cancer Center have an institutional financial conflict of interest with Affimed GmbH. K.R. participates on the Scientific Advisory Board for GemoAb, AvengeBio, Virogin Biotech, GSK, Caribou Biosciences, Navan Technologies and Bayer. N.V. is a founder of CellChorus. The remaining authors declare no competing interests.

Additional information

Extended data is available for this paper at https://doi.org/10.1038/s41591-022-02003-x.

Supplementary information The online version contains supplementary material available at https://doi.org/10.1038/s41591-022-02003-x.

Correspondence and requests for materials should be addressed to Katayoun Rezvani.

Peer review information *Nature Medicine* thanks Adelheid Cerwenka, Nathan Singh and Evan Weber for their contribution to the peer review of this work. Primary Handling Editors: Saheli Sadanand and Joao Monteiro, in collaboration with the *Nature Medicine* team.

Reprints and permissions information is available at www.nature.com/reprints.